Palaeogeography, Palaeoclimatology, Palaeoecology 650 (2024) 112380

Contents lists available at ScienceDirect

Palaeogeography, Palaeoclimatology, Palaeoecology

journal homepage: www.elsevier.com/locate/palaeo

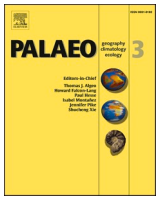

Norian (Upper Triassic) carbon isotopic perturbations and conodont biostratigraphy from the Simao terrane, eastern Tethys

Qiangwang Wu [a], Xin Jin [b], Viktor Karádi [c], Yixing Du [b], Zhiqiang Shi [b,**], Ying Nie [d], Xiang Zhang [b], Angela Bertinelli [e], Manuel Rigo [a,f,*]

[a] Department of Geosciences, University of Padova, 35131 Padova, Italy
[b] State Key Laboratory of Oil and Gas Reservoir Geology and Exploitation and Key Laboratory of Deep-time Geography and Environment Reconstruction and Applications of Ministry of Natural Resources, Chengdu University of Technology, 610059 Chengdu, China
[c] Department of Palaeontology, Institute of Geography and Earth Sciences, Eötvös Loránd University, Pázmány Péter sétány 1/c, Budapest H-1117, Hungary
[d] School of Geoscience and Technology, Southwest Petroleum University, 610500 Chengdu, China
[e] Department of Physics and Geology, University of Perugia, 06123 Perugia, Italy
[f] IGG-CNR, 35131 Padova, Italy

ARTICLE INFO

Editor: S Shen

Keywords:
Upper Triassic
Conodont biostratigraphy
Carbon-isotope
Yunnan province

ABSTRACT

The Norian "chaotic carbon episode" stands out as a compelling carbon cycle perturbation event within the Late Triassic period. This episode has been documented in marine stratigraphic sections across North America, Italy, Japan, and China. However, limited Norian chronostratigraphy available in the eastern Tethys inhibited the identification of this event in this broad area, and thus the possible global response to this carbon cycle perturbation. To address this issue, we analyzed the conodonts and carbon-isotope of the Norian Sanhedong (SHD) section in the Simao terrane, Southwest China. The identification of the Alaunian *Epigondolella spiculata* Zone has well documented the base of the Alaunian stage. Moreover, a conodont faunal turnover can be recognized at the base of the Alaunian, with the evolution of *Mockina* from *Ancyrogondolella* and *Epigondolella*, and it is characterized by a gradual decrease in specimen size. The *E. spiculata* conodont Zone from the SHD section correlates well with the homonymous conodont Zones documented in both the Tethys and the Panthalassa Oceans. Two carbon-isotope negative excursions (CIE1 and CIE2) have also been recorded in the Lacian to Alaunian of the SHD section that can be compared with coeval global sections.

1. Introduction

The Late Triassic is a key period in Earth History, characterized by the initial break-up of the Pangaea supercontinent (e.g., Golonka et al., 2018), significant global climatic fluctuations (e.g., Preto et al., 2010; Trotter et al., 2015; Tanner, 2018; Maron et al., 2024), episodes of faunal turnovers/extinctions (e.g., Mazza et al., 2010; Trotter et al., 2015; Lucas, 2018; Rigo et al., 2020), and perturbations in the carbon cycle (e.g., Zaffani et al., 2017, 2018; Rigo et al., 2020; Jin et al., 2022a; Rigo et al., 2024). These major events are intricately interrelated, making the Late Triassic a time interval of profound environmental and biotic changes. Most notable during this period was the Carnian Pluvial Episode (CPE) (e.g., Furin et al., 2006; Kolar-Jurkovšek and Jurkovšek, 2010; Shi et al., 2019; Tomimatsu et al., 2021, 2023; Jin et al., 2022c, 2023), the Norian/Rhaetian Boundary (Maron et al., 2015; Bertinelli et al., 2016; Rigo et al., 2020, 2024), and the end-Triassic mass extinction (ETME) (e.g., McRoberts and Newton, 1995; Marzoli et al., 2004; Whiteside et al., 2010; Du et al., 2020a; Hua et al., 2023; Todaro et al., 2023), all of them considered to be associated with Large Igneous Provinces (LIPs).

The Norian, the longest stage of the Phanerozoic, spans approximately 21.6 Ma and is characterized by several carbon cycle perturbations of varying magnitudes. Notable perturbations occur at the Carnian/Norian boundary (e.g., Brusatte et al., 2008; Onoue et al., 2016b; Jin et al., 2019; Dal Corso et al., 2020) and at the Norian/Rhaetian boundary (e.g., Rigo et al., 2016, 2020, 2024; Zaffani et al., 2017; Jin et al., 2022a). Recent studies have also identified several carbon-isotopic excursions within the Norian stage at the boundary of

* Corresponding author at: Department of Geosciences, University of Padova, Padova 35131, Italy.
** Corresponding author.
E-mail addresses: szqcdut@163.com (Z. Shi), manuel.rigo@unipd.it (M. Rigo).

https://doi.org/10.1016/j.palaeo.2024.112380
Received 6 May 2024; Received in revised form 11 July 2024; Accepted 14 July 2024
Available online 15 July 2024

Alaunian and Sevatian and in the Sevatian (e.g., Whiteside and Ward, 2011; Zaffani et al., 2017, 2018; Jin et al., 2022a; Sato et al., 2023). These carbon cycle perturbation intervals have been termed the Norian "chaotic carbon interval" (sensu Whiteside and Ward, 2011). Although the identification of several carbon-isotope perturbations during the Norian period (Fig. 1), the mechanisms inducing these perturbations remain inadequately understood. Various hypotheses have been proposed to explain these anomalies, including the eruption of the Angayucham Large Igneous Provinces (LIPs) (Zaffani et al., 2017, 2018; Rigo et al., 2020; Jin et al., 2022b) and the Manicouagan impact event (Sato et al., 2010, 2013, 2016, 2023; van Soest et al., 2011; Rigo et al., 2020).

So far, most records of the Norian carbon-isotope are derived from the middle to upper Norian strata of western Tethys and Panthalassa Ocean (e.g., Whiteside and Ward, 2011; Muttoni et al., 2004, 2014; Onoue et al., 2016a; Zaffani et al., 2017; Sato et al., 2023). These carbon-isotope curves are usually calibrated using conodont zonation frameworks established in British Columbia (Orchard, 1991b, 2018) and Europe (Rigo et al., 2018). In contrast, frequent documentation of Norian conodont zones has only recently started in the eastern Tethys, specifically in the Baoshan terrane (Du et al., 2020b; Jin et al., 2022a; Zeng et al., 2023) and Xizang (Tibet) (Wu et al., 2021, 2023; Lyu et al., 2024). For the Simao terrane, only a lower Norian conodont assemblage has been established in the Sanhedong Formation from the Mojiang area (Wen et al., 2011), with three lower Norian (Lacian) conodont species reported from the same strata in the Weishan area (Wu et al., 2022). Furthermore, carbon-isotope data from this region have yet to be published. The scarcity of Norian conodont and carbon-isotope research hampers the identification of the Norian global carbon cycle perturbation and its correlation with other contemporaneous sections. Therefore, establishing high-resolution conodont biostratigraphy and chemostratigraphy in the eastern Tethys is of key importance.

In the present study, we dedicated to the conodont biostratigraphy and carbon-isotope ($\delta^{13}C$) stratigraphy analysis in the Sanhedong section. Meanwhile, comparing the new Norian carbon-isotope curves from the Sanhedong section with global contemporaneous curves can help to better understand the causes of the Norian-age carbon cycle perturbations in the eastern Tethys and the trigger for the global chaotic carbon episode characterizing the early to middle Norian.

2. Geological setting

The Simao terrane is located in the south-central part of the Sanjiang suture belt and sandwiched between the Lancang River suture belt and the Jinsha River-Ailao Mountain suture belt (Fig. 2). As an important part of the east Tethys tectonic zone, there are two main tendencies in the understanding of the geotectonic position and basin properties of the Simao terrane: one view is that with the subduction suture of the Lancang River Ocean and the Jinsha River Ocean on both sides, its basin properties is (post-arc) foreland basin (Pan et al., 2006). Another view is that the Late Triassic Lanping-Simao region entered the continental margin rift stage (Que et al., 1998; Chen et al., 2004). In terms of geotectonic, the Simao terrane is bordered by the Yangtze Plate to the east and adjacent by the Baoshan terrane to the west (Fig. 2); inferred

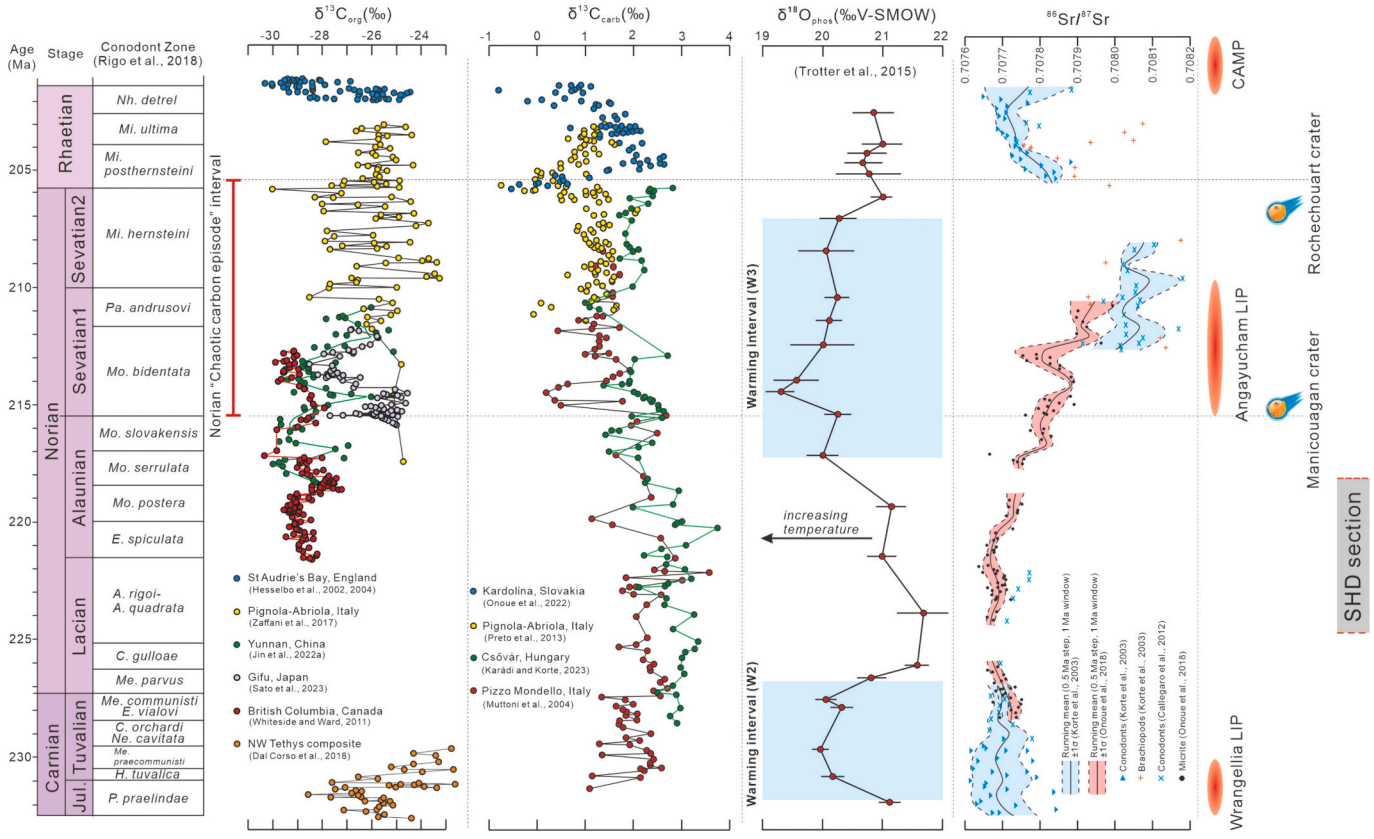

Fig. 1. Upper Triassic time scale (Maron et al., 2019; Ogg et al., 2020) with conodont biostratigraphy (Rigo et al., 2018), $\delta^{13}C_{org}$ (Hesselbo et al., 2002, 2004; Whiteside and Ward, 2011; Zaffani et al., 2017; Dal Corso et al., 2018; Jin et al., 2022a; Sato et al., 2023), $\delta^{13}C_{carb}$ (Muttoni et al., 2004, 2014; Preto et al., 2013; Onoue et al., 2022; Karádi and Korte, 2023), $\delta^{18}O_{phos}$ (Trotter et al., 2015), and $^{87}Sr/^{86}Sr$ (Korte et al., 2003; Callegaro et al., 2012; Onoue et al., 2018) records. Three Large Igneous Provinces (LIPs): Wrangellia (Greene et al., 2010), Angayucham (Ernst and Buchan, 2001; Prokoph et al., 2013), and Central Atlantic Magmatic Province (CAMP; Hesselbo et al., 2002; Blackburn et al., 2013) and two large impact events: Rochechouart (Cohen et al., 2017) and Manicouagan (Jaret et al., 2018) have been reported from the Late Triassic. Abbreviations: *A.* = *Ancyrogondolella*; *C.* = *Carnepigondolella*; *E.* = *Epigondolella*; *H.* = *Hayashiella*; *Me.* = *Metapolygnathus*; *Mi.* = *Misikella*; *Mo.* = *Mockina*; *Pa.* =*Parvigondolella*; *Pr.* = *Primatella*; *Ne.* = *Neocavitella*; *Nh.* = *Neohindeodella*.

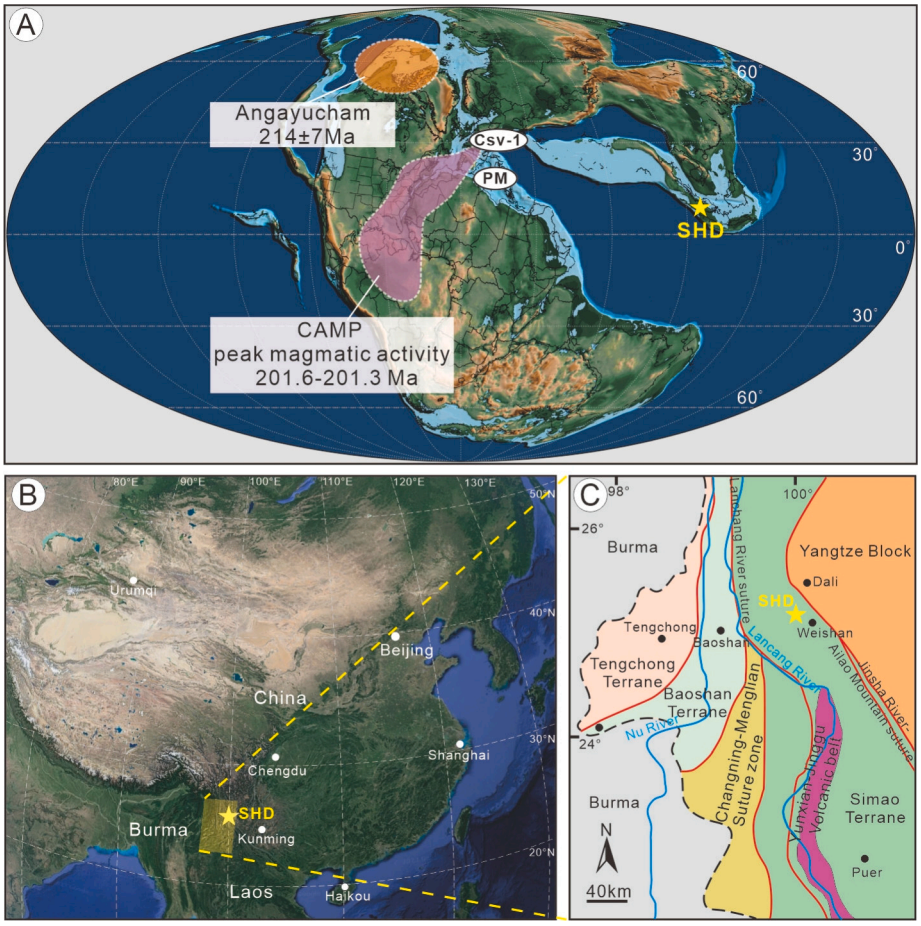

Fig. 2. (A): Paleogeographic map of the Late Triassic (modified from Scotese, 2021) showing the approximate locations of the Angayucham LIP (Sussman and Weil, 2004), the Central Atlantic Magmatic Province (CAMP; Hesselbo et al., 2002; Blackburn et al., 2013), and the position of the Sanhedong section in the eastern Tethys. (B): Map shows the relative position of the study area in southwestern Yunnan, China (modified from Google Earth). (C): Location of the Sanhedong (SHD) section within the Simao terrane (after Deng et al., 2014). Abbreviations: SHD = Sanhedong section; Csv-1 = Csővár core; PM = Pizzo Mondello section.

that the Simao terrane is essentially from the Gondwana, India (Usuki et al., 2013; Wang et al., 2014; Huang and Opdyke, 2016; Yang et al., 2018). During the Devonian-Early Permian, with the opening of the Paleo-Tethys Ocean, the Simao terrane became an independent terrane, which was separated by the Ailao Mountain-Jinsha River Ocean and Changning-Mengliang Ocean, and the overall tectonic pattern is characterized by the alternating distribution of relatively active ocean basins and relatively stable land blocks (Liao et al., 2003). The Simao basin has undergone a multicycle tectonic evolution process, and the geological structure is extremely complex (Wang et al., 2014). The magmatic activity in the basin is mainly controlled by long-term active large faults, and there is strong activity in both the Mesozoic and Cenozoic eras (Deng et al., 2014). The Mesozoic magmatic activities in the Simao basin were dominated by intermediate-acid magmatic rocks and lavas from the Indosinian and Yanshanian volcanic activities, distributed along the Jinsha River-Ailao Mountain fault zone and the Lancang River fault zone (Metcalfe, 2006). The formation of modern basins and the distribution of magmatic rock belts are mainly controlled by thrust overturning and strike-slip structures (Tong, 2018).

The Sanhedong section is located 20 km northwest of Weishan County (Fig. 2). It is composed of the Waigucun Formation, Sanhedong Formation, and Waluba Formation in order. The Sanhedong Formation is mainly characterized by grey to dark grey limestone, bioclastic limestone, dolomitic limestone, and conformity contact with both the overlying Waluba Formation (black shale) and the underlying Waigucun Formation. As a preliminary biostratigraphic study, Wu et al. (2022) reported a lower Norian (Lacian) conodont fauna from the same location and assigned it to the genus *Epigondolella*.

3. Materials and methods

3.1. Conodont sampling and extraction

We collected 44 carbonate rock samples from the SHD section for biostratigraphic investigations (Fig. 3). Individual samples weighing about 3 kg were crushed into approximately 3 cm fragments before being dissolved in formic acid (7%) for 10–15 days. After treatment, the collected residues were washed, sieved (100 μm), and oven-dried at 40 °C. The pre-treatment and dissolution of carbonate rock was carried out at the School of Materials and Chemistry & Chemical Engineering, Chengdu University of Technology. Afterward, the conodont-bearing residues were separated by sodium polytungstate and manually picked using the binocular microscope at the Department of Geosciences, University of Padova. The micrographs of specimens were taken by a scanning electron microscope at the State Key Laboratory of Oil and Gas Reservoir Geology and exploitation and deposited in the Institute of Sedimentary Geology, Chengdu University of Technology.

3.2. Carbonate carbon ($\delta^{13}C_{carb}$) and oxygen ($\delta^{18}O_{carb}$) isotopic analysis

Ninety-three bulk carbonate rock samples were collected for $\delta^{13}C$ investigations. Stable isotope analyses were conducted on carbonate of ca. 0.2–2 mg of powders extracted using a dental drill from freshly broken limestone surfaces (avoiding veins). And then weighted the

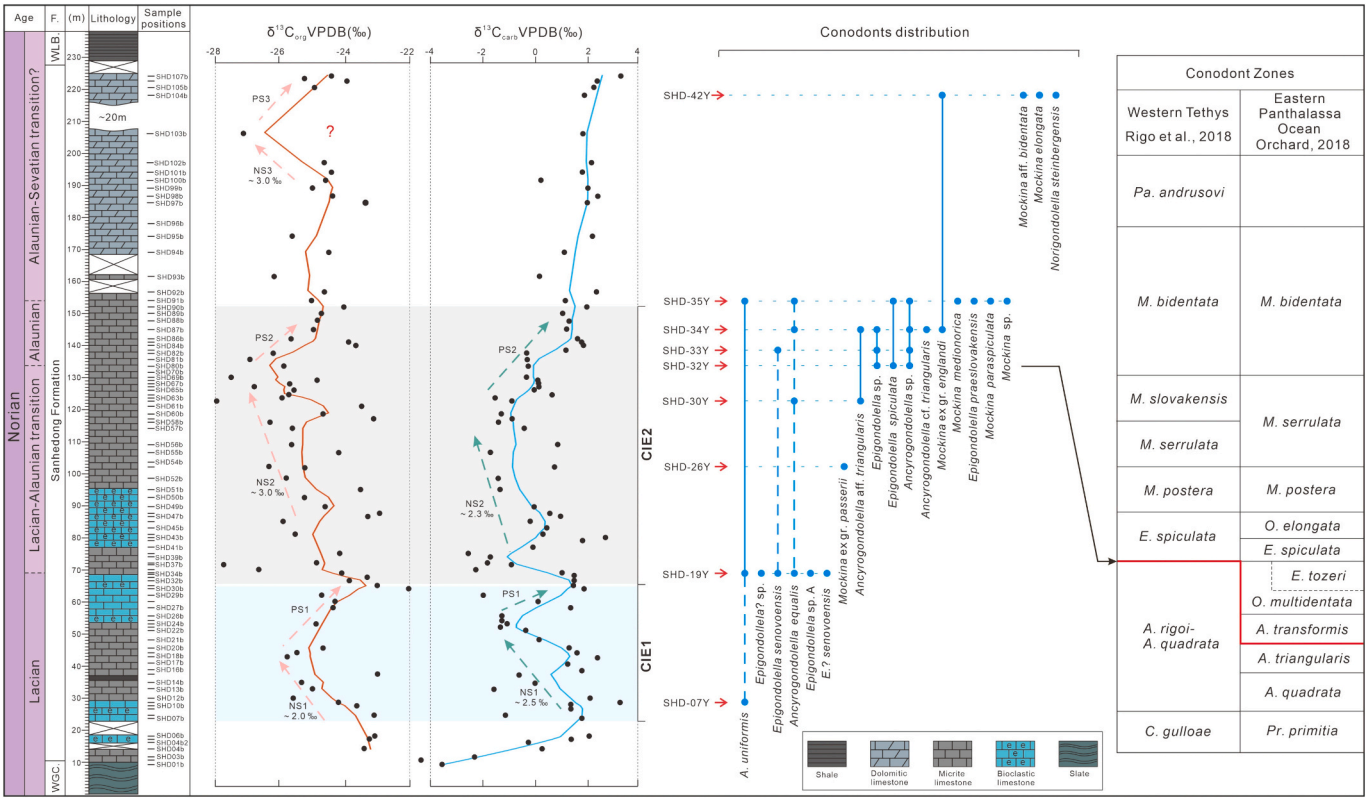

Fig. 3. Logs of the Sanhedong section (update after Wu et al., 2022) with lithostratigraphy, organic carbon isotopes ($\delta^{13}C_{org}$), carbonate carbon isotopes ($\delta^{13}C_{carb}$), and conodont biostratigraphy. The fitting smooth curves (orange and blue lines) were made using locally weighted scatterplot smoothing (LOWESS). Abbreviations: *A.* = *Ancyrogondolella*; *C.* = *Carnepigondolella*; *E.* = *Epigondolella*; *M.* = *Mockina*; *O.* = *Orchardella*; *Pa.* =*Parvigondolella*; *Pr.* = *Primatella*; CIE = Carbon-isotope excursion; PS = positive shift of $\delta^{13}C$ values; NS = negative shift of $\delta^{13}C$ values; F. = Formation; WGC. = Waigucun Formation; WLB. = Waluba Formation. (For interpretation of the references to colour in this figure legend, the reader is referred to the web version of this article.)

obtained powders into exetainer vials. Carbon dioxide (CO_2) was generated at a temperature of 70 °C through the exhaustive reaction with H_3PO_4 exceeding 99%, employing a Gasbench II apparatus connected to a Thermo Delta V Advance isotopic ratio mass spectrometer, located at the Department of Geosciences, University of Padova.

For calibration to the VPDB scale, two internal calcite standards, namely MAQ 1 (with $\delta^{13}C$ of +2.58‰ and $\delta^{18}O$ of −1.15‰) and SUPP (with $\delta^{13}C$ of −49.69‰ and $\delta^{18}O$ of −16.38‰), were utilized. A quality control standard (GR1, Triassic marble from the Monzoni contact aureole) was included in the analysis alongside the samples. The results demonstrate a reproducibility is better than 0.1‰ (1σ) for both carbon and oxygen measurements.

3.3. Organic carbon isotopic ($\delta^{13}C_{org}$) analysis

Seventy-seven bulk rock samples were prepared and washed with deionized water, drying at 50° in an oven, and grinding in an agate mortar. About 2 g of each sample were transferred to polypropylene Falcon tubes that were previously cleaned with 10% HCl and rinsed with deionized water. Between 0.5 and 10 mg of each sample powder were weighed in tin capsules and sealed. The carbon isotopic composition of the samples was measured using a Thermo Scientific Delta V Advantage Isotopic Ratio Mass Spectrometer (IRMS) coupled to a Thermo Scientific Flash 2000 Elemental Analyzer (EA) at the University of Padova. The international standards CH-6 ($\delta^{13}C$ = −10.449 ‰ VPDB) and CH-7 ($\delta^{13}C$ = −32.151 ‰ VPDB) were used for calibration and normalization. An internal standard ZER ($\delta^{13}C$ = −25.99±0.24 ‰ VPDB) was also used for quality control, and the precision was checked, which was better than +/− 0.15 ‰ (standard deviation).

4. Conodont biostratigraphy and carbon isotope results

4.1. Conodont biostratigraphy

The lowermost part of the Sanhedong section (about 28.5 m, sample SHD-07Y) is less productive. Only one conodont species, *Ancyrogondolella* cf. *uniformis*, was recovered from this level (Figs. 3 and 4). The species was first described in the Lacian ammonoid *Malayites dawsoni* Zone in British Columbia, Canada (Orchard, 1991a). The species *A. uniformis* has been extensively documented in various regions, including the eastern Panthalassa Ocean (Orchard, 1991a, 2006, 2018), the Tethyan area, and specifically in Slovakia (Channell et al., 2003), Italy (Mazza et al., 2010, 2012b; Mazza and Martínez-Pérez, 2015; Rigo et al., 2018), Hungary (Karádi, 2018; Karádi and Korte, 2023), and Xizang, China (Wu et al., 2023; Lyu et al., 2024). *Ancyrogondolella uniformis* was found in the *A. triangularis* Zone, which was usually assigned to the upper Lacian in both British Columbia (e.g., Orchard, 1991a, 2018) and Europe (Kozur, 2003; Moix et al., 2007). In the Xizang region, the *A. uniformis* Zone was used to contrast with the *A. triangularis* Zone owing to the absence of *A. triangularis* species. It was assigned to the upper Lacian (Wu et al., 2023; Lyu et al., 2024). In addition, the range of *A. uniformis* possibly extends to the Alaunian (Mazza et al., 2012b; Karádi et al., 2021).

In the interval from 69 m to 122.9 m (samples SHD-19Y, 26Y, 30Y), the conodont fauna is characterized by the occurrence and dominance of *Ancyrogondolella uniformis*, *Epigondolella*? sp., *E.*? *senovoensis*, *A. equalis*, *A.*? cf. *equalis*, *Epigondolella* sp. A, *E. senovoensis*, *Mockina* ex gr. *passerii*, and *A.* aff. *triangularis*, among them, *Epigondolella*? sp., *Epigondolella* sp. A and *E.*? *senovoensis* are only present in sample SHD-19Y (Figs. 4–6). However, both *E. senovoensis* and *A. equalis* have a wide range from 69 m

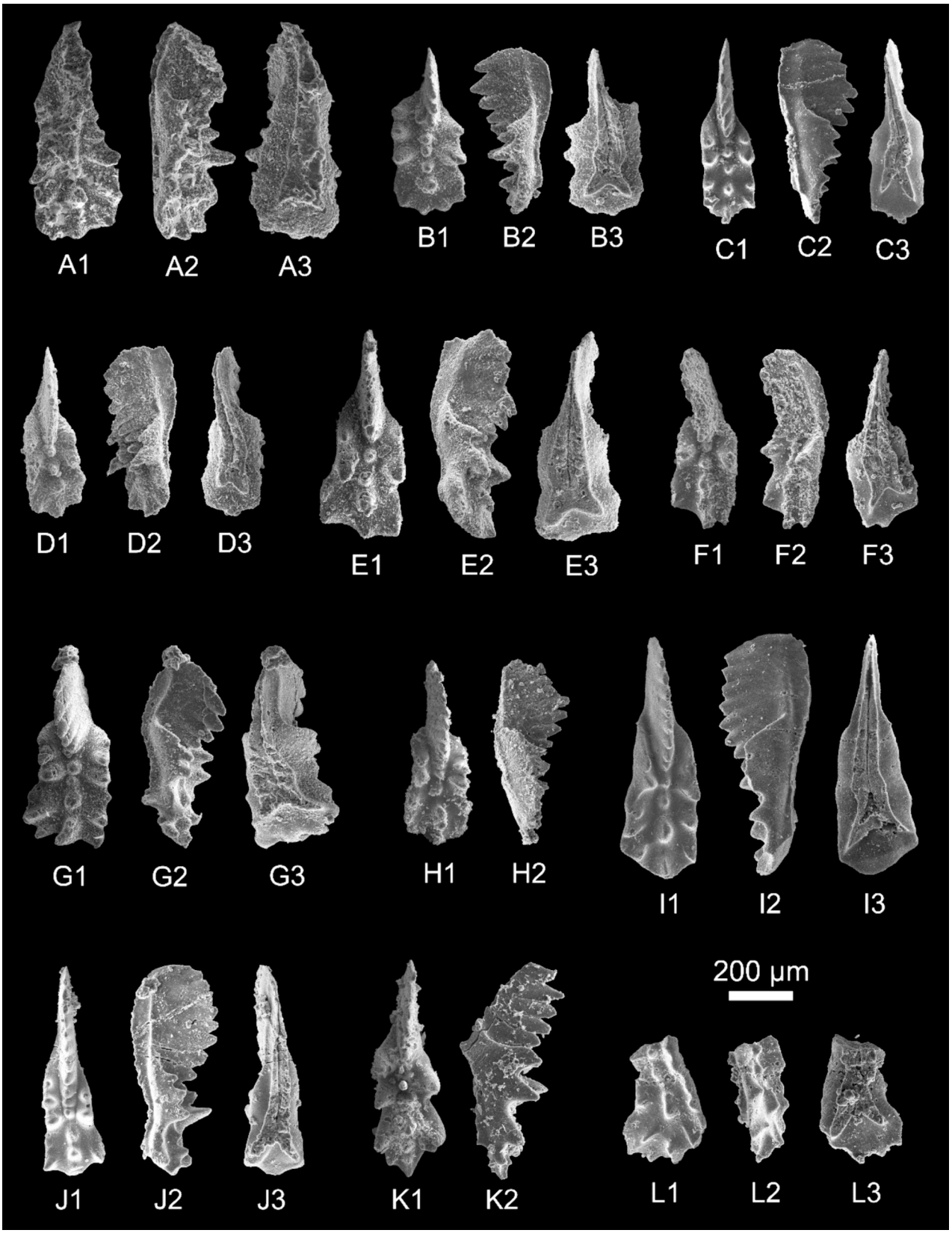

Fig. 4. SEM micro-photographs of conodonts of the Sanhedong section. The scale bar is 200 μm and all specimens are on the same scale. 1: upper view, 2: lateral view, 3: lower view. A). *Ancyrogondolella* cf. *uniformis*, sample SHD-07Y; B, C). *Ancyrogondolella uniformis*, B: sample SHD-19Y, C: sample SHD-35Y; D). *Epigondolella*? sp., sample SHD-19Y; E). *Epigondolella*? *senovoensis*, sample SHD-19Y; F). *Epigondolella senovoensis*, sample SHD-33Y; G). *Ancyrogondolella equalis*, sample SHD-19Y; H). *Ancyrogondolella*? cf. *equalis*, sample SHD-30Y; I, J). *Ancyrogondolella equalis*?, I: sample SHD-34Y, J: sample SHD-35Y; K). *Mockina* ex gr. *passerii*, sample SHD-26Y; L). *Ancyrogondolella* cf. *triangularis*, sample SHD-34Y.

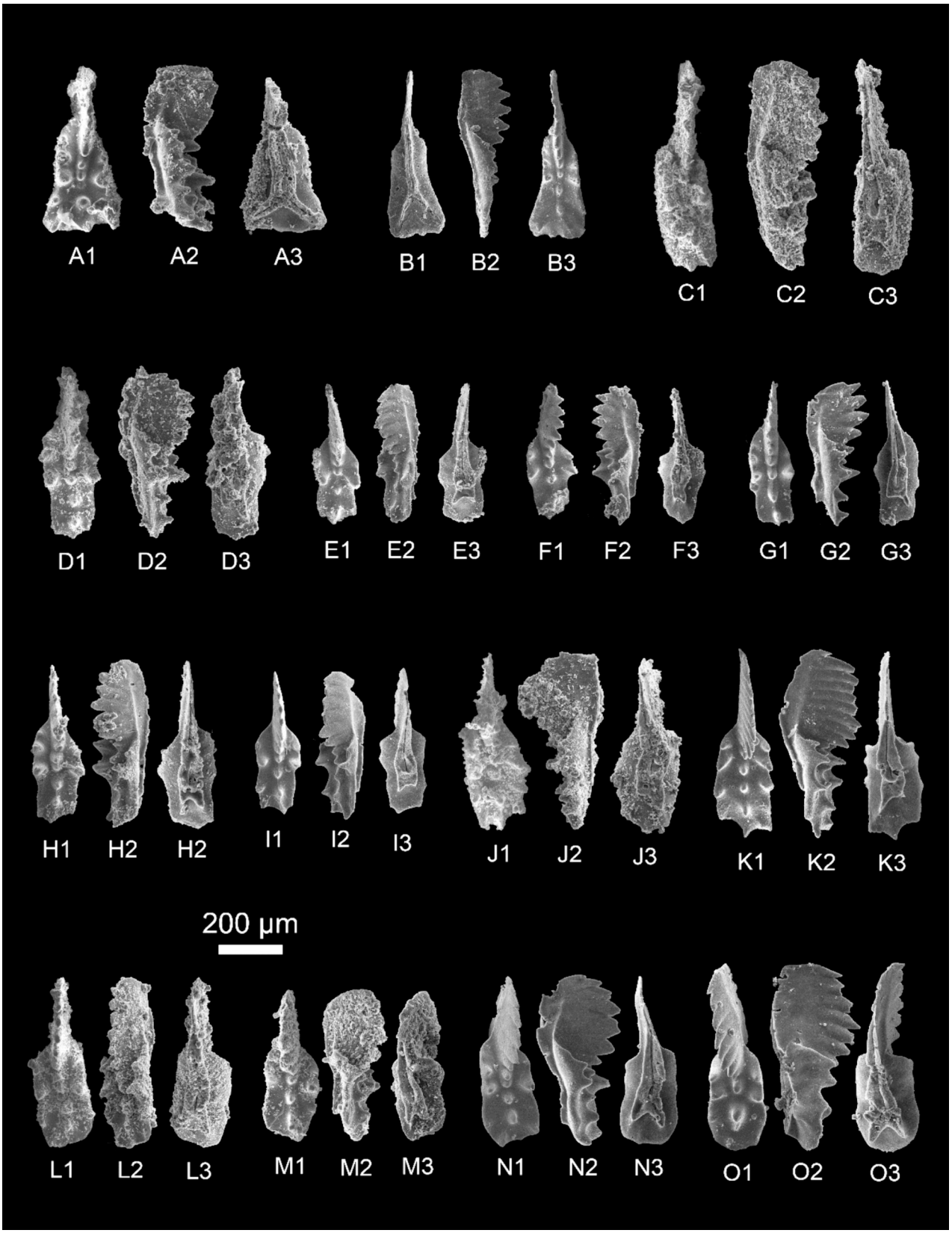

Fig. 5. SEM micro-photographs of conodonts of the Sanhedong section. The scale bar is 200 μm and all specimens are on the same scale. 1: upper view, 2: lateral view, 3: lower view. A, B). *Ancyrogondolella* aff. *triangularis*, A: sample SHD-30Y, B: sample SHD-34Y; C-I). *Epigondolella* sp., C, D: sample SHD-32Y, E, F, H, I: sample SHD-33Y, G: sample SHD-34Y; J, K). *Epigondolella spiculata*, J: sample SHD-32Y, K: sample SHD-35Y; L-O). *Ancyrogondolella* sp., L: sample SHD-32Y, M: sample SHD-33Y, N, O: sample SHD-34Y.

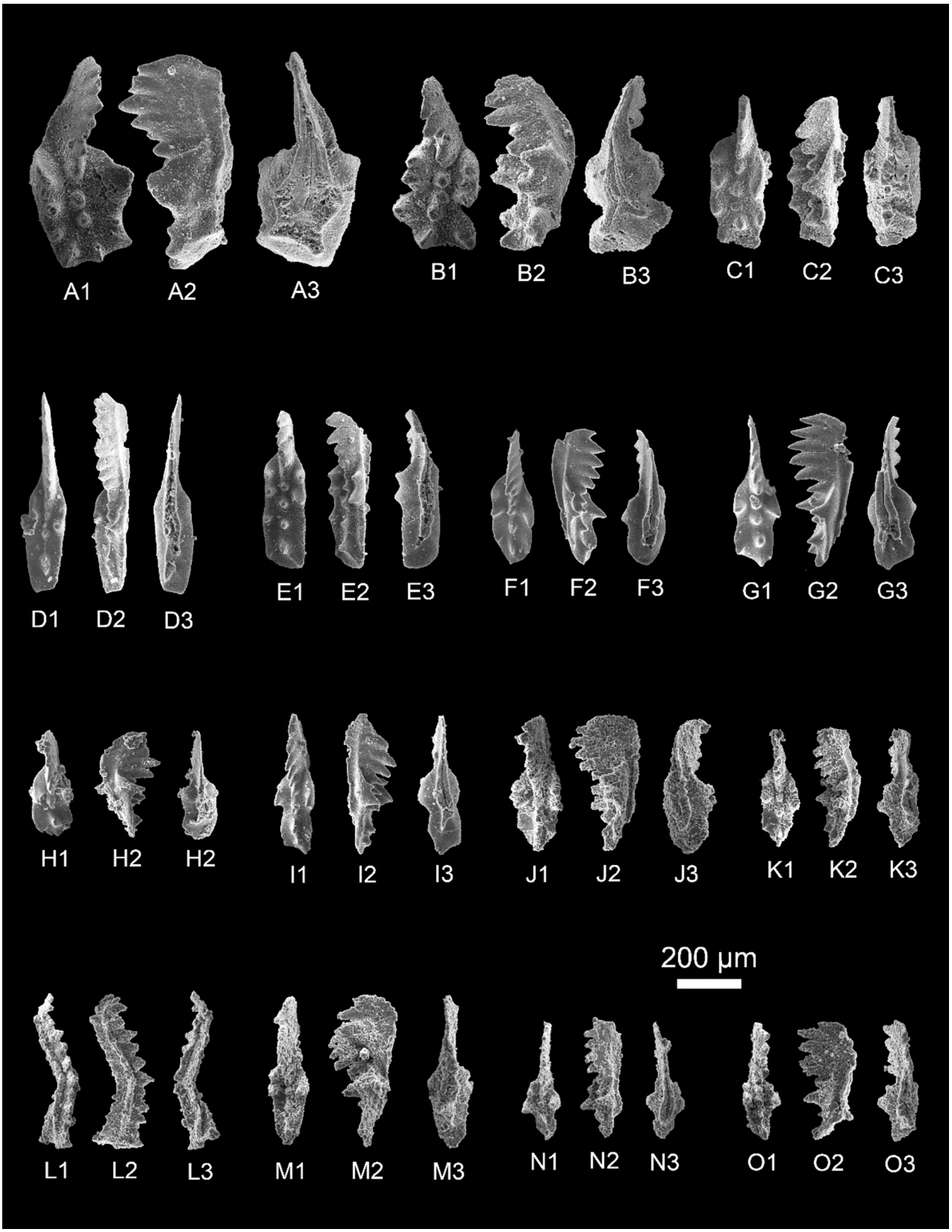

Fig. 6. SEM micro-photographs of conodonts of the Sanhedong section. The scale bar is 200 μm and all specimens are on the same scale. 1: upper view, 2: lateral view, 3: lower view. A). *Epigondolella* sp. A, sample SHD-19Y; B). *Epigondolella*? *senovoensis*, sample SHD-19Y; C). *Epigondolella*? sp., sample SHD-19Y; D). *Mockina medionorica*, sample SHD-35Y; E). *Mockina* sp., sample SHD-35Y; F). *Mockina* ex gr. *englandi*, sample SHD-34Y; G). Subadult *Epigondolella* sp., sample SHD-35Y; H). *Epigondolella praeslovakensis*, sample SHD-35Y; I). *Mockina paraspiculata*, sample SHD-35Y; J, K). *Mockina* ex gr. *englandi*, sample SHD-42Y; L). *Norigondolella steinbergensis*, sample SHD-42Y; M). *Mockina elongata*, sample SHD-42Y; N, O). *Mockina* aff. *bidentata*, sample SHD-42Y.

(sample SHD-19Y) to 138.7 m (sample SHD-33Y) and 154 m (sample SHD-35Y), respectively. The species *A.* aff. *triangularis* is distributed between 122.9 m and 145 m. The species *E. senovoensis* was first described in the upper part of the Lacian-Alaunian transition and the Alaunian 1 of the Dovško Section, Slovenia (Karádi et al., 2021). *Ancyrogondolella equalis* has been reported from the Lacian-Alaunian transitional interval of the eastern Panthalassa Ocean (Orchard, 2018). Meanwhile, it is also present in the Lacian to Alaunian of Tethyan sections, such as Hungary (Karádi and Korte, 2023), Slovenia (Karádi et al., 2021), and Xizang, China (Lyu et al., 2024), where it prevalently accompanies *A. uniformis* or appears above it. Only one poorly preserved conodont specimen was recovered from SHD-26Y that was assigned to the species *M.* ex gr. *passerii*, which was first described by Jin et al. (2022a) from the Sevatian strata of Yunnan, China, but an earlier first occurrence is possible. The *Ancyrogondolella triangularis-Norigondolella hallstattensis* Zone in the Tethys region has been proposed to correlate with the *A. triangularis* Zone, which established by Orchard (1991b, 2018) in the eastern Panthalassa Ocean (Channell et al., 2003; Moix et al., 2007), and both zones were considered to be the last of conodont zone of the upper Lacian in the respective region (Orchard, 1991b, 2018; Moix et al., 2007). Karádi (2018) studied the *A. triangularis* in Hungary (western Tethys) and suggested that it is a characteristic lower Norian species. In eastern Tethys, the species *A. triangularis* is rarely reported (Wu et al., 2023; Lyu et al., 2024), and only a few *A.* aff. *triangularis* specimens were presented by Wu et al. (2022) in the Sanhedong section from western Yunnan. Since a large number of conodont specimens with transitional characters towards the Alaunian faunas are found in the SHD-19Y to SHD-30Y interval, we designate this interval as the Lacian-Alaunian transition.

In the strata interval spanning from 134 m to 154 m, the sample SHD-32Y has been found to yield specimens of *Epigondolella* sp., *E. spiculata*, *Ancyrogondolella* sp. Notably, the species *E. spiculata* was first identified by Orchard (1991a) from middle Norian strata of the Canadian Cordillera and has been reported extensively from various regions, including eastern Panthalassa Ocean (Katvala and Stanley Jr., 2008; Orchard, 2018; Lei et al., 2022; Fucelli et al., 2023), western Tehtys (Rigo et al., 2005; Balini et al., 2010; Karádi, 2018, 2021; Rigo et al., 2018), eastern Tethys (Ji et al., 2003; Wu et al., 2023; Lyu et al., 2024), and Central Panthalassa Ocean (Yamashita et al., 2018). The species has been found to occur across the Alaunian, excluding the uppermost Alaunian strata (Karádi, 2018). Rigo et al. (2018) proposed the designation of *E. spiculata* as the index species for the lower Alaunian. Therefore, we selected the first occurrence (FO) of *E. spiculata* as the mark of the base of Alaunian in the Sanhedong section, even if its base might be stratigraphically extended downwards due to the absence of conodont-rich fauna below its first occurrence. The last occurrence (LO) of *E. senovoensis* is documented in sample SHD-33Y and accompanied by species *Epigondolella* sp. and *Ancyrogondolella* sp. The sample SHD-34Y is characterized by the LO of *A.* aff. *triangularis* and *Epigondolella* sp., and the FO of *Mockina* ex gr. *englandi*. The species *M. englandi* was defined by Orchard (1991a) as an upper Norian species from the Canadian Cordillera. Afterward, an abundance of specimens of *M. englandi* has been reported in various sections worldwide (Orchard et al., 2007a, 2007b; Mazza et al., 2012a, 2012b; Du et al., 2020b; Caruthers et al., 2022; Karádi and Korte, 2023; Lei et al., 2024; Zeng et al., 2023; Lyu et al., 2024), and its range extends from the upper Norian to Rhaetian. The sample SHD-35Y is characterized by the presence of *M. medionorica*, *E. praeslovakensis*, *M. paraspiculata*, and *Mockina* sp. Instead, *Ancyrogondolella uniformis*, *A. equalis*?, *E. spiculata*, and *Ancyrogondolella* sp. last occur at this level. The species *M. medionorica* was previously identified in the Alaunian of the western Tethys (Kovács and Kozur, 1980; Vrielynck, 1987; Channell et al., 2003; Kozur, 2003; Karádi, 2018; Karádi et al., 2021) and of the central Panthalassa Ocean (Ishida and Hirsch, 2001). Successively, Zeng et al. (2023) reported some specimens in the lower Sevatian of the Madoupo section in Baoshan terrane, Yunnan (eastern Tethys), suggesting that it has a longer range (from the lower Alaunian to Sevatian) and wider distribution. The species *E. praeslovakensis* was considered the forerunner of *M. slovakensis* (Moix et al., 2007), which is frequently encountered in the middle to upper Alaunian and documented in diverse marine settings (Moix et al., 2007; Rigo et al., 2018; Du et al., 2021a; Jin et al., 2022a; Lyu et al., 2024). In addition, the species *M. paraspiculata* was first described in the Alaunian *Mockina postera-Norigondolella steinbergensis* fauna in the strata of the South Qiangtang terrane (Wu et al., 2023).

From the sample SHD-42Y, the conodont fauna is dominated by *Mockina* aff. *bidentata*, *Mockina* ex gr. *englandi*, *M. elongata*, and *Norigondolella steinbergensis*. It is noteworthy that *Mockina* aff. *bidentata* present at the top of the SHD section appears to be the subadult of *M. bidentata*, which is a marker species for the upper Norian, so this species requires careful identification (Orchard, 1983; Orchard, 1991a; Mazza and Martínez-Pérez, 2015; Chen et al., 2016; Rigo et al., 2018; Lyu et al., 2024). The species *M. elongata* has been reported worldwide (Orchard, 1991a; Rigo et al., 2005; Yamashita et al., 2018; Zeng et al., 2023), and it has a stratigraphic range from the middle Alaunian to lower Sevatian. Moreover, the cosmopolitan species *N. steinbergensis* was documented in different places (Ishida and Hirsch, 2001; Channell et al., 2003; Orchard et al., 2007b; Mazza et al., 2010; Rigo et al., 2016; Kolar-Jurkovšek and Jurkovšek, 2019; Du et al., 2020b; Karádi et al., 2021; Wu et al., 2021, 2023; Karádi and Korte, 2023; Zeng et al., 2023; Lyu et al., 2024), and has a wide range from middle Norian to late Rhaetian. However, genus *Norigondolella* was temperature dependent, preferring cold water environments (Trotter et al., 2015).

4.2. Carbonate carbon isotope

Carbon isotope data was generated from 93 bulk carbonate samples, and the results of $\delta^{13}C_{carb}$ are present in Fig. 3 together with lithology, $\delta^{13}C_{org}$, and conodont biostratigraphy. The carbon curve generally shows an increasing trend, and the $\delta^{13}C_{carb}$ values range of 7.36‰ and fluctuate between −4.26 and 3.1‰ (Fig. 3). Among them, a short-term positive and negative fluctuation is presented in the 23-152 m interval with two negative excursions and a stable increasing trend zone from 120 m to the top. The most negative values of the $\delta^{13}C_{carb}$ were observed at the base of this section, reaching approximately −4‰ (Fig. 3). Due to the lack of data at this horizon, it is not possible to determine whether this was a significant negative carbon isotope excursion event. The first negative excursion (CIE1) was observed between 23 and 66 m in the Lacian, and the amplitude of the $\delta^{13}C_{carb}$ values was about 2.5‰ (Fig. 3). The second negative excursion (CIE2) occurred in the 66–152 m interval, and which is composed of about 2.3‰ decrease in $\delta^{13}C_{carb}$ values.

4.3. Organic carbon isotope

A total of 77 buck rock samples were analyzed for the organic carbon isotope ($\delta^{13}C_{org}$) of bulk organic matter. The $\delta^{13}C_{org}$ values vary from −27.90 ‰ to −22.08 ‰ in the studied section (Fig. 3). Although the $\delta^{13}C_{org}$ curve does not show a significant trend as a whole, two carbon-isotope excursions are recognized (CIE1 and CIE2 in Fig. 3). The lowest $\delta^{13}C_{org}$ isotopic excursion (CIE1) is observed at 23 m to 66 m, and which is composed of a ~ 2.0‰ decrease in $\delta^{13}C_{org}$ values within the Lacian. The second $\delta^{13}C_{org}$ isotopic excursion (CIE2) consists of a ~ 3.0‰ long-term negative shift and short positive shift across the Lacian-Alaunian transition to Alaunian from 66 m to 153 m, with three slight carbon isotope oscillations (Fig. 3). Subsequently, a potential CIE can be observed at the top of the Sanhedong section from 190 m to 225 m. However, a few valid data points and the absence of the age-diagnostic conodont species limited the identification of the CIE, so we placed a question mark on this interval (Figs. 3 and 9).

5. Discussion

5.1. Global correlation of the Norian conodont biostratigraphy

The Upper Triassic conodont biozonations established in British Columbia (eastern Panthalassa Ocean, Orchard, 1991a, 1991b) and Europe (western Tethys, Rigo et al., 2018) have been extensively applied in global stratigraphic comparisons. The correlation between the two zonations is evident based on certain characteristic species, including the Lacian *Ancyrogondolella quadrata*, the Alaunian *Epigondolella spiculata*, *Mockina postera*, and *M. serrulata*, as well as the lower Sevatian species *M. bidentata*. Among these, Lacian conodont species have received more extensive study compared to the Alaunian and Sevatian species due to their proximity to the Carnian/Norian boundary (CNB), as observed at the Norian GSSP in the Pizzo Mondello section of Sicily, Italy (Mazza et al., 2010; Mazza et al., 2012a, 2012b, 2018; Rigo et al., 2012b, 2018; Karádi et al., 2013; Onoue et al., 2018; Hounslow et al., 2021), as well as at an important CNB section at Black Bear Ridge in British Columbia, Canada (Orchard, 2014, 2018, 2019; Hounslow et al., 2021). In the eastern Tethys region of China, only a few Norian conodont species have been reported, primarily due to the limited distribution of Norian marine strata (Wang and Dong, 1985; Mao and Tian, 1987; Ji et al., 2003; Dong and Wang, 2006; Wang and Lang, 2019; Du et al., 2020b; Tong et al., 2021; Lyu et al., 2024). In recent years, Norian conodont associations have been described frequently in the Baoshan terrane of Yunnan (Wang et al., 2019; Du et al., 2020b; Jin et al., 2022a, 2022b, 2022c; Zeng et al., 2021, 2023), as well as Banggong-Nujiang suture, North Qiangtang block, and South Qiangtang block of Xizang (Wu et al., 2021, 2023; Lyu et al., 2024). The abundance of specimens recovered during the present study enables the initial documentation of the conodont zones from the Lacian to the upper Alaunian in strata of the Simao terrane (Fig. 7). The *E. spiculata* Zone identified in the SHD section prove strong correlation to the previously established conodont zones in the eastern Tethys, specifically within the North Qiangtang block (Lyu et al., 2024) and Lhasa block (Mao and Tian, 1987; Ji et al., 2003). Additionally, this zone also correlates well with the western Tethys zones (Rigo et al., 2018) and eastern Panthalassa Ocean zones (Orchard, 2018). Therefore, the new study of the Norian conodont biostratigraphy in the Simao terrane supports the stratigraphic comparisons among the microcontinents in eastern Tethys and also contributes to correlating the western Tethys, eastern Panthalassa Ocean, and central Panthalassa Ocean regions in terms of both in stratigraphy and conodont faunal evolution.

5.1.1. The base of the Alaunian (middle Norian) within the Sanhedong section

In the Tethys regions, the common use of open nomenclature and an oversimplified approach to defining conodont species, coupled with the inadequate illustration of lower and mid-Alaunian specimens, have significantly impacted the definition and subdivision of the Alaunian substage within conodont biozones (e.g. Channell et al., 2003; Bertinelli et al., 2005; Mazza et al., 2012a; Rigo et al., 2012b; Karádi, 2021). The base of the Alaunian is previously suggested by the FO of the ammonoid species *Cyrtopleurites bicrenatus* (Kozur, 2003; Lucas, 2010). Successively, Kozur (2003) introduced the conodont species *Mockina medionorica*, designating it as the index species for the homonymous biozone from western Tethys. This Tethyan biozone was correlated to the eastern Panthalassa Ocean *Orchardella multidentata* Zone, which was established by Orchard (1991a) at the base of the Alaunian. However, the recognition of *M. medionorica* poses challenges due to its holotype is only

<table>
<tr><td>Western Tethys</td><td>Eastern Panthalassa Ocean</td><td>Central Panthalassa Ocean</td><td colspan="6">Eastern Tethys</td></tr>
<tr><td rowspan="2">European</td><td rowspan="2">British Columbia</td><td rowspan="2">Japan</td><td colspan="4">Xizang</td><td colspan="2">Yunnan</td></tr>
<tr><td>Lhasa</td><td>S. Qiangtang</td><td>N. Qiangtang</td><td>BNS</td><td>Baoshan</td><td>Simao</td></tr>
<tr><td>Rigo et al., 2018</td><td>Orchard, 2018</td><td>Yamashita et al., 2018</td><td>Mao et al., 1987
Ji et al., 2003</td><td>Wu et al., 2023</td><td>Lyu et al., 2024</td><td>Wu et al., 2021</td><td>Wang & Dong , 1985
Jin et al., 2022
Zeng et al., 2023</td><td>Present study</td></tr>
<tr><td>Mi. hernsteini</td><td rowspan="2"></td><td rowspan="2"></td><td rowspan="2"></td><td rowspan="3"></td><td rowspan="3"></td><td rowspan="9"></td><td></td><td rowspan="4"></td></tr>
<tr><td>Pa. andrusovi</td><td>Pa. andrusovi</td></tr>
<tr><td>M. bidentata</td><td>M. bidentata</td><td>M. bidentata</td><td>M. bidentata</td><td>M. bidentata</td></tr>
<tr><td>M. slovakensis</td><td rowspan="3">M. serrulata</td><td rowspan="3">M. postera</td><td rowspan="3">M. postera</td><td rowspan="3">M. postera-Ne. steinbergensis</td><td>M. slovakensis</td></tr>
<tr><td>M. serrulata</td><td>M. serrulata</td><td rowspan="2">M. postera</td></tr>
<tr><td>M. postera</td><td>M. postera</td><td>M. postera</td></tr>
<tr><td>E. spiculata</td><td>O. elongata</td><td rowspan="6">A. triangularis</td><td rowspan="2">E. spiculata</td><td rowspan="2"></td><td>O. elongata</td><td rowspan="4"></td><td rowspan="4"></td><td>E. spiculata</td></tr>
<tr><td>E. spiculata</td><td>E. spiculata</td><td rowspan="3"></td><td rowspan="3"></td></tr>
<tr><td rowspan="5">A. rigoi-A. quadrata</td><td>E. tozeri</td></tr>
<tr><td>O. multidentata</td><td rowspan="2">A. uniformis-N. hallstattensis</td><td>A. uniformis</td></tr>
<tr><td>A. transformis</td><td rowspan="3"></td><td rowspan="3">A. rigoi-A. quadrata- N. hallstattensis</td></tr>
<tr><td>A. triangularis</td></tr>
<tr><td>A. quadrata</td><td rowspan="2">A. quadrata</td></tr>
<tr><td>C. gulloae</td><td>Pr. primitia</td><td></td><td></td><td></td><td></td><td></td></tr>
</table>

Fig. 7. Reported conodont zonation of the Norian stage in China and its global correlation. Conodont successions from different sections or areas are presented, but it should be noted that exact age equivalence is not implied. Abbreviations: *A.* = *Ancyrogondolella*, *C.* = *Carnepigondolella*, *E.* = *Epigondolella*, *M.* = *Mockina*, *Mi.* = *Misikella*, *O.* = *Orchardella*, *Pa.* = *Parvigondolella*, *Pr.* = *Primatella*; BNS = Bangong-Nujiang Suture Zone.

illustrated from the upper view (Kozur, 2003, pl. 1, Fig. 5), and its occurrence is sporadic (Moix et al., 2007; Rigo et al., 2018). Hence, the species *Epigondolella spiculata* has been suggested as the index species for the lower Alaunian by Rigo et al. (2018) rather than *M. medionorica* since *E. spiculata* is early recognizable and it occurs in both Tethys realm and eastern Panthalassa Ocean (Ji et al., 2003; Rigo et al., 2005, 2012b; Karádi, 2018; Orchard, 1991a, 2018; Lyu et al., 2024). It is noteworthy that some specimens previously described as *E. multidentata* from both Yunnan (Wang and Dong, 1985; Dong and Wang, 2006) and Xizang (Mao and Tian, 1987) are now reassigned to species *E. spiculata* (Orchard, 2018; Karádi, 2018, 2024). Therefore, it is recommended to discontinue the use of the previously established *E. multidentata* Zone in Yunnan areas (Fig. 7).

The definition of index species for the base of the Alaunian in both the eastern Panthalassa Ocean and Tethys is currently controversial (Rigo et al., 2018; Orchard, 2018; Lyu et al., 2024). Rigo et al. (2018) recommended using *Epigondolella spiculata* as an index species for the lower Alaunian in the Tethys realm, and it was later used in Xizang, China (Lyu et al., 2024). However, in the eastern Panthalassa Ocean, two conodont zones *Ancyrogondolella transformis* Zone and *Orchardella multidentata* Zone (with *E. tozeri* Subzone), have been established by Orchard (2018) under *E. spiculata* Zone in the lower Alaunian, and the base of the *A. transformis* Zone provides an easily recognizable datum for defining the Lacian/Alaunian boundary. Both critical species of the middle Norian, *Mockina medionorica* and *E. spiculata*, are found in the present study. Since species *M. medionorica* has some of the shortcomings mentioned before. Therefore, we decided to use the FO of *E. spiculata* as the marker of the base of the Alaunian because it is the first surely Alaunian conodont species in the SHD section, similarly in other Tethys regions (Rigo et al., 2018; Lyu et al., 2024).

In addition, a rapid conodont morphological radiation and faunal turnover event has been recorded from different regions at the Lacian-Alaunian boundary interval (Orchard, 2018; Karádi et al., 2020; Lyu et al., 2024). Norian conodont faunas are usually characterized by the dominance of the genera *Epigondolella* and *Mockina*. Orchard (2018) reveals intricate details of the evolutionary path of conodont morphological changes within a remarkably thin stratigraphic interval from the Pardonet Formation of northeast British Columbia (Canada), which is characterized by the morphological transition from genera *Ancyrogondolella* with a bifid keel to other genera with not bifurcated keel, including *Mockina*, *Orchardella*, and *Epigondolella*. Karádi et al. (2020) described that the evolution of Norian conodonts was characterized by a retrograde phase starting from the Lacian-Alaunian boundary interval. This evolution came also along with the increase in juvenile mortality of middle Norian conodonts in the Tethys realm, which was suggested to be linked to environmental perturbations (Karádi, 2018; Karádi et al., 2020). A similar phenomenon of juvenile dominance was reported in both the Chaiwei and Tuoba sections from the North Qiangtang block, where a significant conodont faunal turnover from *Ancyrogondolella* to *Epigondolella* was also recorded between the Lacian and Alaunian (Lyu et al., 2024).

In the present study, the beginning of the faunal transition from *Ancyrogondolella* and *Epigondolella* to *Mockina* in the lower part of the Alaunian in the Sanhedong section has been discovered, which coincides with the similar phenomenon reported from the eastern Panthalassa Ocean (Orchard, 2018) and eastern Tethys (Lyu et al., 2024). In addition, it is visible in Fig. 6 that the descendants of the genus *Ancyrogondolella* show a significant reduction in size from the Lacian-Alaunian transition to the top of the SHD section. This evolutionary trend was documented and discussed in detail previously by Karádi (2021). However, the factors that influenced the conodont evolution during this period are currently unresolved, and more endeavor is needed in the future (Karádi et al., 2020).

5.2. Diagenetic screening of Norian stable carbon isotopes

The original $\delta^{13}C_{carb}$ value of the bulk carbonate may potentially be influenced by diagenesis. It is necessary to rule out diagenetic alteration effectively before interpreting the carbon isotope data from ancient rocks (Preto et al., 2013; Swart, 2015; Jin et al., 2018, 2022a). Currently, various techniques can be employed to determine whether diagenesis has modified the original $\delta^{13}C_{carb}$ signal, encompass petrographic analysis, the correlation between $\delta^{13}C_{carb}$ and $\delta^{18}O_{carb}$, Mn/Sr ratios, and the examination of dolomitization (Du et al., 2022). The $\delta^{13}C_{carb}$ composition of the Sanhedong section exhibits a primary or near-primary marine carbonate signature, as inferred from the follows: (1) the analyzed powder was obtained using a microdrill, carefully sampled from fresh micritic limestone, with a deliberate effort to avoid weathering areas and veins; (2) no observable indications of subaerial exposure or notable dissolution-reprecipitation processes; (3) crossplots show the lack of covariation between $\delta^{13}C_{carb}$ and $\delta^{18}O_{carb}$ ($R = 0.05$; Fig. 8A) suggesting a weak influence of meteoric or burial diagenesis on the analyzed samples (Algeo et al., 1992; Cramer and Jarvis, 2020); (4) $\delta^{13}C_{carb}$ and $\delta^{13}C_{org}$ varied consistently in the upper Lacian and lower-middle Alaunian (Fig. 3) and were moderately correlated (Fig. 8B), suggesting that both originated from the original seawater dissolved inorganic carbon reservoir (DIC) and preserved $\delta^{13}C$ fluctuations of the DIC; (5) the $\delta^{13}C_{carb}$ value fluctuates between −4.26 and 3.1‰ (Fig. 3), most of them are similar to other global reference $\delta^{13}C_{carb}$ value of the Norian (Muttoni et al., 2004, 2014; Preto et al., 2013; Karádi and Korte, 2023).

In contrast to $\delta^{13}C_{carb}$, the carbon isotopic composition of organic matter ($\delta^{13}C_{org}$) is relatively resistant to diagenetic fractionation (e.g. Jin et al., 2019, 2022a).

5.3. Global correlation of the Norian $\delta^{13}C$ records

The $\delta^{13}C$ stratigraphy has emerged as the principal stable isotopic methodology for chronostratigraphic correlation within the pre-Cenozoic epochs of Earth's history, as evidenced by its comprehensive documentation of positive and negative excursions (Saltzman and Thomas, 2012). The $\delta^{13}C$ values of carbonates have been widely utilized as reliable proxies for the reconstruction of seawater chemistry, climate, and marine productivity and for exploring global carbon cycle dynamics through geologic time (Cramer and Jarvis, 2020; Jin et al., 2022a). Additionally, the carbon-isotope record of the Earth's history serves as a useful tool for stratigraphic correlation (Cramer and Jarvis, 2020).

Extensive studies have reported $\delta^{13}C$ records from the upper Norian in the Panthalassa Ocean and Tethys regions. Whiteside and Ward (2011) first documented a continuous $\delta^{13}C_{org}$ record spanning the Alaunian-Sevatian substages within the Frederick Island (FI) section in British Columbia, Canada. They identified a pronounced negative excursion with a magnitude of ca. 2.5‰ within the Alaunian upper *H. columbianus* Zone (Fig. 1). This zone corresponds to the upper Alaunian conodont *M. serrulata* Zone (Orchard, 1991a, 2018). Similarly, Onoue et al. (2016a) reported a CIE at the boundary between the Alaunian *Mockina postera* Zone and the Sevatian *M. bidentata* Zone, which correlates with the radiolarian 6A and 6B Zones. This negative shift coincides with the Manicouagan impact event (Onoue et al., 2016a; Jaret et al., 2018; Sato et al., 2023). Additionally, Zaffani et al. (2017) reconstructed the global $\delta^{13}C_{org}$ profile of the upper Norian sediments, identifying three negative excursions in the Lagonegro Basin. Furthermore, Jin et al. (2022a) documented the organic and carbonate carbon-isotope trends in the Hongyan-B section of Baoshan terrane (western Yunnan), specifically covering the Alaunian *M. slovakensis* Zone and the Sevatian *M. bidentata* Zone. Sato et al. (2023) also reported a CIE in the Sevatian conodont *M. bidentata* Zone (equivalent to the radiolarian TR7 and TR8A Zones). All these CIE events occur within the Norian "chaotic carbon episode" interval. However, these CIEs cannot be identified in the SHD section due to the absence of Sevatian age-diagnostic species

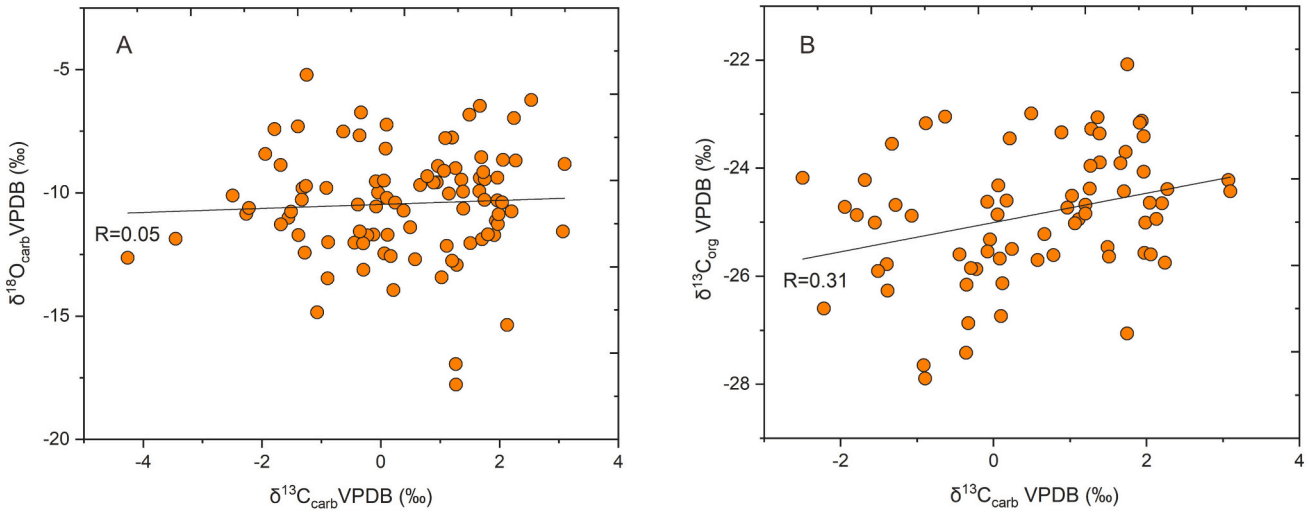

Fig. 8. Crossplots of stable isotope analyses from the Sanhedong section. (A) $\delta^{13}C_{carb}$-$\delta^{18}O_{carb}$, R = 0.05; (B) $\delta^{13}C_{carb}$-$\delta^{13}C_{org}$, R = 0.31.

based on the conodont biostratigraphy (Figs. 3 and 9).

In the present study, we first described two Norian negative carbon-isotope excursions (CIEs) in the Lacian to Alaunian of the SHD section from the eastern Tethys region (Figs. 3 and 9). Based on the conodont biostratigraphy, these CIEs can be correlated with the two continuous carbon-isotope curves reported by Muttoni et al. (2004, 2014) and

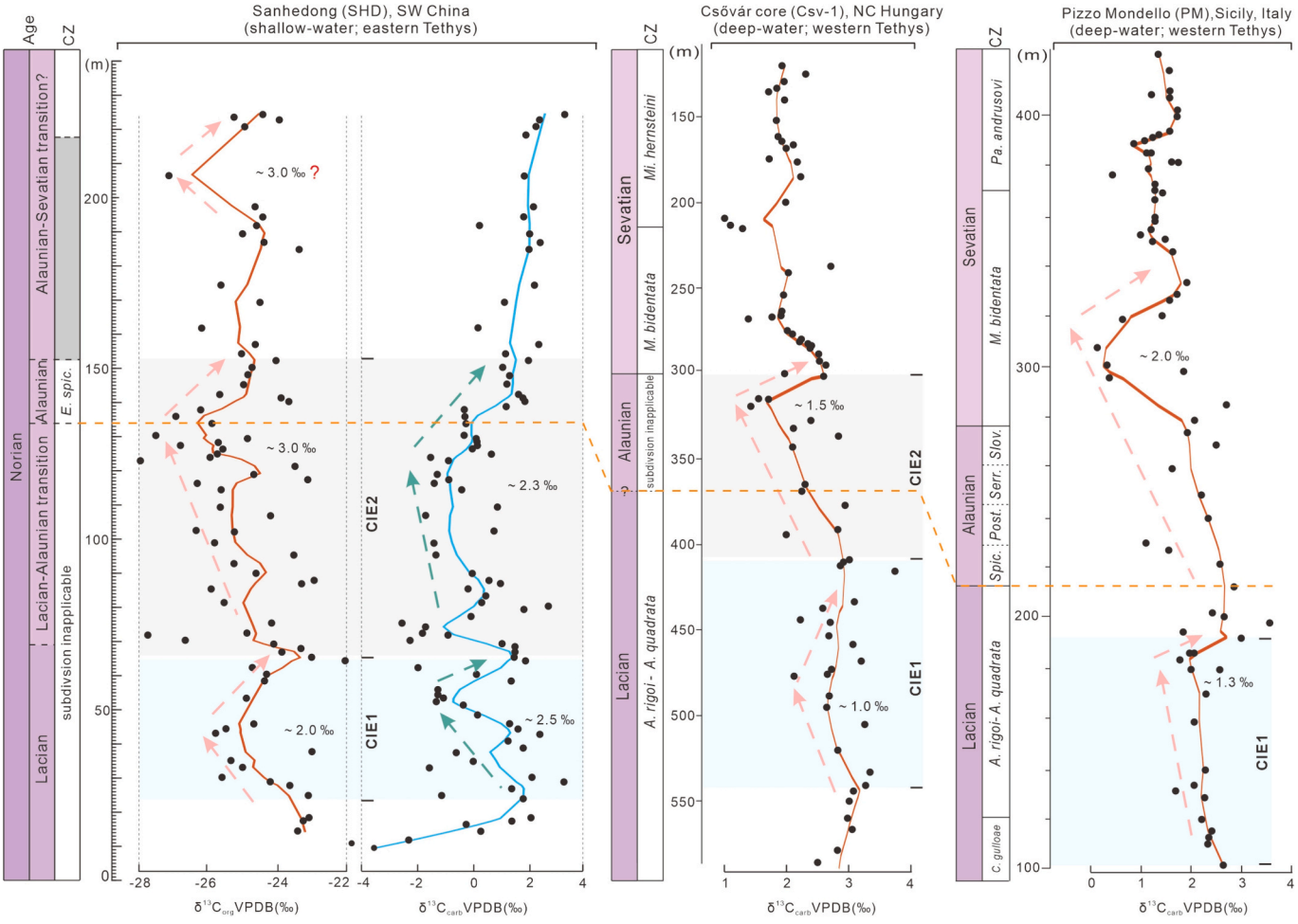

Fig. 9. Comparison of the $\delta^{13}C$ record based on the conodont biostratigraphy from the Sanhedong section with those from the Csővár core (Hungary; Karádi and Korte, 2023) and Pizzo Mondello section (Sicily, Italy; Muttoni et al., 2004, 2014). The approximate locations of the inferred depositional areas of these sections are plotted on the Late Triassic paleogeographic map (Fig. 2A). The fitting smooth curves were made using locally weighted scatterplot smoothing (LOWESS). Conodont zones of the PM section present *Spic*. for *M. spiculata*, *Post*. for *M. postera*, *Serr*. for *M. serrulata*, and *Slov*. for *M. slovakensis* biozones. Abbreviations: CZ = conodont zones.

Karádi and Korte (2023) from the western Tethys (Fig. 9), respectively. The first negative carbon-isotope excursion (CIE1) of the SHD section ranges from 23 m to 66 m, which is comparable to a CIE with an amplitude of ca. 1.0‰ at 410 m to 545 m in the Csővár core and a CIE with an amplitude of ca. 1.3‰ at 100 m to 195 m in the Pizzo Mondello (PM) section, both in the Lacian conodont *A. rigoi-A. quadrata* Zone (Fig. 9). The second negative carbon-isotope excursion (CIE2) of the SHD section occurred in the 66–152 m interval and corresponded to the CIE2 of the Csővár core, with an amplitude of ca. 1.5‰ and ranging across the Lacian-Alaunian boundary interval. However, this CIE2 is not recorded in the PM section, which may be ascribed to the lower sampling resolution (Fig. 9). It should be noted that the CIE2 from the SHD section and Csővár core both are characterized by the long-term negative shift following a sharp positive shift (Fig. 9). The CIE1 and CIE2 in the Lacian and Alaunian, as documented in the SHD section, Csővár core, and PM section from the different sedimentary environments (e.g. Gullo, 1996; Wu et al., 2022; Karádi and Korte, 2023), may suggest a global carbon cycle perturbation during the early to middle Norian (Fig. 9).

5.4. The causes of the Norian carbon-isotopic excursions

The $\delta^{18}O_{phos}$ curve from biogenic apatite in the Tethyan region (Rigo and Joachimski, 2010; Rigo et al., 2012a; Trotter et al., 2015; Du et al., 2021b) indicates that an intense sea-surface warm event (marked "W3" in Fig. 1) occurred during the middle to late Norian. This event is characterized by a temperature increase of approximately 6 °C (~1.5‰) in sea-surface waters. Elevated global temperatures have the potential to destabilize methane clathrates on the seafloor, releasing substantial quantities of previously sequestered carbon and leading to markedly negative $\delta^{13}C$ values in the global ocean, thereby contributing to an overall decline in global ocean $\delta^{13}C$ (Zaffani et al., 2017; Rigo et al., 2020, 2024; Lei et al., 2021). Furthermore, the substantial increase in $^{87}Sr/^{86}Sr$ values from the lower to upper Norian is commonly considered to be the outcome of increased weathering intensity caused by the rapid uplift of the Cimmeride-Indosinian orogens, marking the closure of the Palaeotethys (Korte et al., 2003; Onoue et al., 2018). The pronounced release of greenhouse gases (CO_2, CH_4) from volcanic activity may contribute to global warming, which in turn accelerates the global hydrological cycle and thus enhances weathering. This is another way to interpret the increase in $^{87}Sr/^{86}Sr$ values (Onoue et al., 2018; Jin et al., 2022a). The emplacement of Angayucham large igneous province (LIP) is currently identified as a main factor triggering the Norian "chaotic carbon episode" (Zaffani et al., 2017; Rigo et al., 2020, 2024; Jin et al., 2022a; Sato et al., 2023), supported by $\delta^{18}O_{phos}$ profile (Trotter et al., 2015), $^{87}Sr/^{86}Sr$ curve (Korte et al., 2003; Onoue et al., 2018; Lei et al., 2022), and *Re*-Os isotope values (Sato et al., 2023). However, biostratigraphic constraints suggest that the CIE1 and CIE2 observed in this study occur in the Lacian to Alaunian (Fig. 9), thereby ruling out the effects of the Angayucham LIP (214 ± 7 Ma; Ernst and Buchan, 2001; Prokoph et al., 2013) during this interval. Moreover, large extraterrestrial impacts have also been considered as a potential cause of the Norian CIE events in the Late Triassic (Onoue et al., 2016a; Rigo et al., 2020). However, the Manicouagan impact event (215.5 ± 1 Ma; Jaret et al., 2018) and the Rochechouart impact event (206.92 ± 0.32 Ma; Cohen et al., 2017; Sato et al., 2021), occurred in the late Norian. Therefore, these impact events cannot be the triggers of CIE events recorded in early to middle Norian (Fig. 9).

The early to middle Norian CIE events were first described in this study, However, the sparse published carbon-isotope data from this interval hampers broader global correlation and mechanistic investigations of the early to middle Norian CIE events. Therefore, further investigation is essential to establish high-resolution conodont biostratigraphy in the eastern Tethys. Additionally, a comprehensive search for isotopic stratigraphy constrained by biostratigraphy is needed for improved global comparisons.

6. Conclusions

An integrated study of conodont biostratigraphy and carbon-isotope ($\delta^{13}C$) analysis from the Sanhedong (SHD) section in the Simao terrane of western Yunnan Province, SW China, has provided valuable insights into carbon-isotope excursions and their correlation with global records. The Alaunian *Epigondolella spiculata* conodont Zone has been identified. Based on conodont biostratigraphy, the base of the Alaunian has been provisionally placed at meter 134 (SHD-32Y). Furthermore, we first described two negative carbon-isotope excursions (termed CIE1 and CIE2) in the SHD section from the eastern Tethys. Notably, these CIEs, occurring in the Lacian to Alaunian, exhibit global correlatability. However, additional research is needed for comprehensive geochemical and palaeontological studies to better understand the causes of carbon cycle perturbation events during the Norian period.

CRediT authorship contribution statement

Qiangwang Wu: Writing – original draft, Visualization, Methodology, Investigation, Conceptualization. **Xin Jin:** Writing – review & editing, Validation, Resources, Methodology. **Viktor Karádi:** Writing – review & editing, Visualization. **Yixing Du:** Writing – review & editing, Visualization. **Zhiqiang Shi:** Writing – review & editing, Supervision, Resources, Conceptualization. **Ying Nie:** Writing – review & editing. **Xiang Zhang:** Writing – review & editing. **Angela Bertinelli:** Writing – review & editing. **Manuel Rigo:** Writing – review & editing, Supervision, Resources, Conceptualization.

Declaration of competing interest

The authors declare that they have no known competing financial interests or personal relationships that could have appeared to influence the work reported in this paper.

Data availability

Data will be made available on request.

Acknowledgments

We wish to thank Bin Chen, He Yin, Lu Han, Xiaomei Zhou, Yu Ge, Bingyao Hu, Changhao Li, Meiling Wang, and Bao Guo for their help in the sample preparation and fieldwork. We also thank Nereo Preto (University of Padova) for helpful discussions. We are grateful to the editor, Prof. Shuzhong Shen, and two reviewers, Prof. Yanlong Chen and Prof. Tea Kolar-Jurkovšek, for their constructive comments. This research was supported by the University of Padova to Manuel Rigo (No. DOR2348181) and the China Scholarship Council to Qiangwang Wu (No. 202108510027).

Appendix A. Supplementary data

Supplementary data to this article can be found online at https://doi.org/10.1016/j.palaeo.2024.112380.

References

Algeo, T.J., Wilkinson, B.H., Lohmann, K.C., 1992. Meteoric-burial diagenesis of Middle Pennsylvanian limestones in the Orogrande Basin, New Mexico; water/rock interactions and basin geothermics. J. Sediment. Res. 62, 652–670.

Balini, M., Bertinelli, A., Di Stefano, P., Guaiumi, C., Levera, M., Mazza, M., Muttoni, G., Nicora, A., Preto, N., Rigo, M., 2010. The late Carnian-Rhaetian succession at Pizzo Mondello (Sicani Mountains). Albertiana 39, 36–57.

Bertinelli, A., Casacci, M., Concheri, G., Gattolin, G., Godfrey, L., Katz, M.E., Maron, M., Mazza, M., Mietto, P., Muttoni, G., Rigo, M., Sprovieri, M., Stellin, F., Zaffani, M., 2016. The Norian/ Rhaetian boundary interval at Pignola-Abriola section (southern Apennines, Italy) as a GSSP candidate for the Rhaetian stage: an update. Albertiana 43, 6–19.

Bertinelli, A., Ciarapica, G., De Zanche, V., Marcucci, M., Mietto, P., Passeri, L., Rigo, M., Roghi, G., 2005. Stratigraphic evolution of the Triassic–Jurassic Sasso di Castalda succession (Lagonegro basin, Southern Apennines, Italy). Ital. J. Geosci. 124, 161–175.

Blackburn, T.J., Olsen, P.E., Bowring, S.A., McLean, N.M., Kent, D.V., Puffer, J., McHone, G., Rasbury, E.T., Et-Touhami, M., 2013. Zircon U-Pb geochronology links the end- Triassic extinction with the Central Atlantic Magmatic Province. Science 340, 941–945.

Brusatte, S.L., Benton, M.J., Ruta, M., Lloyd, G.T., 2008. Superiority, competition, and opportunism in the evolutionary radiation of dinosaurs. Science 321 (5895), 1485–1488. https://doi.org/10.1126/science.1161833.

Callegaro, S., Rigo, M., Chiaradia, M., Marzoli, A., 2012. Latest Triassic marine Sr isotopic variations, possible causes and implications. Terra Nova 24, 130–135. https://doi.org/10.1111/j.1365-3121.2011.01046.x.

Caruthers, A.H., Marroquín, S.M., Gröcke, D.R., Golding, M.L., Aberhan, M., Them, T.R., Veenma, Y.P., Owens, J.D., McRoberts, C.A., Friedman, R.M., Trop, J.M., Szűcs, D., Pálfy, J., Rioux, M., Trabucho-Alexandre, J.P., Gill, B.C., 2022. New evidence for a long Rhaetian from a Panthalassan succession (Wrangell Mountains, Alaska) and regional differences in carbon cycle perturbations at the Triassic-Jurassic transition. Earth Planet. Sci. Lett. 577 (117262), 14.

Channell, J.E.T., Kozur, H.W., Sievers, T., Mock, R., Aubrecht, R., Sykora, M., 2003. Carnian-Norian biomagnetostratigraphy at Silicka Brezova (Slovakia): correlation to other Tethyan sections and to the Neward Basin. Palaeogeogr. Palaeoclimatol. Palaeoecol. 191, 65–109.

Chen, Y.K., Liao, Z.T., Wei, Z.H., Li, M.H., 2004. Characteristics and tectonic evolution of the Lanping-Simao Mesozoic Basin. Pet. Geol. Exp. 26, 219–222 (in Chinese with English abstract).

Chen, Y., Neaubauer, T.A., Krystyn, L., Richoz, S., 2016. Allometry in Anisian (Middle Triassic) segminiplanate conodonts and its implications for conodont taxonomy. Palaeontology 59, 725–741.

Cohen, B.E., Mark, D.F., Lee, M.R., Simpson, S.L., 2017. A new high-precision $^{40}Ar/^{39}Ar$ age for the Rochechouart impact structure: at least 5 Ma older than the Triassic–Jurassic boundary. Meteorit. Planet. Sci. 52, 1600–1611.

Cramer, B.D., Jarvis, I., 2020. Carbon isotope stratigraphy. In: Geologic Time Scale 2020. Elsevier, pp. 309–343. https://doi.org/10.1016/B978-0-12-824360-2.00011-5.

Dal Corso, J., Gianolla, P., Rigo, M., Franceschi, M., Roghi, G., Mietto, P., Manfrin, S., Raucsik, B., Budai, T., Jenkyns, H.C., 2018. Multiple negative carbon-isotope excursions during the Carnian Pluvial Episode (Late Triassic). Earth Sci. Rev. 185, 732–750.

Dal Corso, J., Bernardi, M., Sun, Y., Song, H., Seyfullah, L.J., Preto, N., Gianolla, P., Ruffell, A., Kustatscher, E., Roghi, G., 2020. Extinction and dawn of the modern world in the Carnian (Late Triassic). Sci. Adv. 6, eaba0099.

Deng, J., Wang, Q., Li, G., Li, C., Wang, C., 2014. Tethys tectonic evolution and its bearing on the distribution of important mineral deposits in the Sanjiang region, SW China. Gondwana Res. 26 (2), 419–437. https://doi.org/10.1016/j.gr.2013.08.002.

Dong, Z.Z., Wang, W. (Eds.), 2006. The Cambrian-Triassic Conodont Faunas in Yunnan, China-Correlative Biostratigraphy and the Study of Palaeobiogeographic Province of Conodont, 128–146. Yunnan Science and Technology Press, Kunming (in Chinese with English abstract).

Du, Y., Chiari, M., Karádi, V., Nicora, A., Onoue, T., Pálfy, J., Roghi, G., Tomimatsu, Y., Rigo, M., 2020a. The asynchronous disappearance of conodonts: new constraints from Triassic/Jurassic boundary sections in the Tethys and Panthalassa. Earth Sci. Rev. 203, 103176.

Du, Y., Bertinelli, A., Jin, X., Shi, Z., Karádi, V., Yin, H., Han, L., Wu, Q., Rigo, M., 2020b. Integrated conodont and radiolarian biostratigraphy of the Upper Norian in Baoshan Block, Southwestern China. Lethaia 53 (4), 533–545. https://doi.org/10.1111/let.12374.

Du, Y., Karádi, V., Roghi, G., Ponton, M., Cozzi, A., Rigo, M., 2021a. Revision of the conodont *Mockina slovakensis* and its paleogeographic implications for the upper triassic intraplatform basins of the alps. J. Earth Sci. 32 (3), 657–666. https://doi.org/10.1007/s12583-021-1411-5.

Du, Y., Onoue, T., Karádi, V., Williams, I.S., Rigo, M., 2021b. Evolutionary process from *Mockina bidentata* to *Parvigondolella andrusovi*: evidence from the Pizzo Mondello Section, Sicily, Italy. J. Earth Sci. 32 (3), 667–676. https://doi.org/10.1007/s12583-020-1362-2.

Du, Y., Zhu, Y.Y., Dal Corso, J., Huang, J.D., Qiu, H.O., Song, H.J., Tian, L., Chu, D.L., Tong, J.N., Song, H.Y., 2022. New early Triassic marine δ13C record from the northeastern Yangtze Platform: implications for contemporaneous temperature changes and volcanic eruptions. Palaeogeogr. Palaeoclimatol. Palaeoecol. 607, 111270 https://doi.org/10.1016/j.palaeo.2022.111270.

Ernst, R.E., Buchan, K.L., 2001. Large mafic magmatic events through time and links to mantle-plume heads. Geol. Soc. Am. Spec. Pap. 352, 483–575.

Fucelli, A., Golding, M., Peybernes, C., Martini, R., 2023. Siliciclastic input controlling carbonate deposition on a low-angle ramp system: New insight from the Upper Triassic Luning Formation (Western-Central Nevada). Sediment. Geol. 450, 106394 https://doi.org/10.1016/j.sedgeo.2023.106394.

Furin, S., Preto, N., Rigo, M., Roghi, G., Gianolla, P., Crowley, J.L., Bowring, S.A., 2006. High-precision U–Pb zircon age from the Triassic of Italy: implications for the Triassic time scale and the Carnian origin of calcareous nannoplankton and dinosaurs. Geology 34, 1009. https://doi.org/10.1130/G22967A.1.

Golonka, J., Embry, A., Krobicki, M., 2018. Late Triassic global plate tectonics. In: The Late Triassic World. Springer, Cham, pp. 27–57. https://doi.org/10.1007/978-3-319-68009-5_2.

Greene, A.R., Scoates, J.S., Weis, D., Katvala, E.C., Israel, S., Nixon, G.T., 2010. The architecture of oceanic plateaus revealed by the volcanic stratigraphy of the accreted Wrangellia oceanic plateau. Geosphere 6, 47–73.

Gullo, M., 1996. Conodont biostratigraphy of uppermost Triassic deep-water calcilutites from Pizzo Mondello (Sicani Mountains): evidence for Rhaetian pelagites in Sicily. Palaeogeogr. Palaeoclimatol. Palaeoecol. 126, 309–323. https://doi.org/10.1016/S0031-0182(96)00043-0.

Hesselbo, S.P., Robinson, S.A., Surlyk, F., Piasecki, S., 2002. Terrestrial and marine extinction at the Triassic-Jurassic boundary synchronized with major carbon-cycle perturbation: a link to initiation of massive volcanism? Geology 30, 251–254.

Hesselbo, S.P., Robinson, S.A., Surlyk, F., 2004. Sea-level change and facies development across potential Triassic–Jurassic boundary horizons, SW Britain. J. Geol. Soc. Lond. 161, 365–379. https://doi.org/10.1144/0016-764903-033.

Hounslow, M.W., Bachmann, G.H., Balini, M., Benton, M.J., Carter, E.S., Konstantinov, A.G., Golding, M.L., Krystyn, L., Kürschner, W.M., Lucas, S.G., McRoberts, C.A., Muttoni, G., Nicora, A., Onoue, T., Orchard, M.J., Ozsvárt, P., Paterson, N.W., Richoz, S., Rigo, M., Sun, Y., Tackett, L.S., Tekin, U.K., Wang, Y., Zhang, Y., Zonneveld, J.P., 2021. The case for the Global Stratotype Section and Point (GSSP) for the base of the Norian Stage. Albertiana 46, 25–57.

Hua, X., Yin, R., Kemp, D.B., Huang, C., Shen, J., Jin, Xin, 2023. Mercury isotope constraints on the timing and pattern of magmatism during the end-Triassic mass extinction. Earth Planet. Sci. Lett. 624, 118438.

Huang, K., Opdyke, N.D., 2016. Paleomagnetism of the Upper Triassic rocks from south of the Ailaoshan Suture and the timing of the amalgamation between the South China and the Indochina Blocks. J. Asian Earth Sci. 119, 118–127. https://doi.org/10.1016/j.jseaes.2015.12.005.

Ishida, K., Hirsch, F., 2001. Taxonomy and faunal affinity of late Carnian-Rhaetian conodonts in the Southern Chichibu Belt, Shikoku, SW Japan. Riv. Ital. Paleontol. Stratigr. 107 (2), 227–250.

Jaret, S.J., Hemming, S.R., Rasbury, E.T., Thompson, L.M., Glotch, T.D., Ramezani, J., Spray, J.G., 2018. Context matters – Ar–Ar results from in and around the Manicouagan Impact Structure, Canada: implications for martian meteorite chronology. Earth Planet. Sci. Lett. 501, 78–89. https://doi.org/10.1016/j.epsl.2018.08.016.

Ji, Z.S., Yao, J.X., Yang, X.D., Zang, W.S., Wu, G.C., 2003. Conodont zonation of Norian in Lhasa area, Xizang (Tibet) and their global correlation. Acta Palaeontol. Sin. 42 (3), 382–392 (in Chinese with English abstract).

Jin, Xin, Shi, Z.Q., Rigo, M., Manfrin, S., Franceschi, M., Preto, N., 2018. Carbonate platform crisis in the Carnian (Late Triassic) of Hanwang (Sichuan Basin, South China): insights from new biostratigraphic and stable isotope data. J. Asian Earth Sci. 164, 104–124.

Jin, X., McRoberts, C.A., Shi, Z., Mietto, P., Rigo, M., Roghi, G., Manfrin, S., Franceschi, M., Preto, N., 2019. The aftermath of the CPE and the Carnian–Norian transition in northwestern Sichuan Basin, South China. J. Geol. Soc. 176 (1), 179–196. https://doi.org/10.1144/jgs2018-104.

Jin, X., Du, Y., Bertinelli, A., Shi, Z., Preto, N., Zou, H., Ogg, J.G., Han, L., Wu, Q., Rigo, M., 2022a. Carbon-isotope excursions in the Norian stage (Upper Triassic) of the Baoshan terrane, western Yunnan, China. J. Asian Earth Sci. 230, 105215 https://doi.org/10.1016/j.jseaes.2022.105215.

Jin, X., Ogg, J.G., Lu, S., Shi, Z., Kemp, D.B., Hua, X., Onoue, T., Rigo, M., 2022b. Terrestrial record of carbon-isotope shifts across the Norian/Rhaetian boundary: a high-resolution study from northwestern Sichuan Basin, South China. Glob. Planet. Chang. 210, 103754 https://doi.org/10.1016/j.gloplacha.2022.103754.

Jin, X., Franceschi, M., Martini, R., Shi, Z.Q., Gianolla, P., Rigo, M., Wall, C.J., Schmitz, M.D., Lu, G., Du, Y.X., Huang, X.T., Preto, N., 2022c. Eustatic sea-level fall and global fluctuations in carbonate production during the Carnian Pluvial Episode. Earth Planet. Sci. Lett. 594, 117698.

Jin, X., Tomimatsu, Y., Yin, R., Onoue, T., Franceschi, M., Grasby, S.E., Du, Y.X., Rigo, M., 2023. Climax in Wrangellia LIP activity coincident with major Middle Carnian (Late Triassic) climate and biotic changes: mercury isotope evidence from the Panthalassa pelagic domain. Earth Planet. Sci. Lett. 607, 118075.

Karádi, V., 2018. Middle Norian Conodonts from the Buda Hills, Hungary: an Exceptional Record from the Western Tethys. J. Iber. Geol. 44, 155–174.

Karádi, V., 2021. Evolutionary trends of the genus *Ancyrogondolella* (Conodonta) and related taxa in the Norian (late Triassic). J. Earth Sci. 32 (3), 700–708.

Karádi, V., 2024. Towards a refined Norian (Upper Triassic) conodont biostratigraphy of the western Tethys: revision of the recurrent 'multidentata-issue'. Geol. Mag. 1–19.

Karádi, V., Korte, C., 2023. Upper Carnian to Rhaetian (Upper Triassic) conodont and carbon-isotope stratigraphy of the Csővár borehole succession, Hungary. Palaeogeogr. Palaeoclimatol. Palaeoecol. 630, 111792 https://doi.org/10.1016/j.palaeo.2023.111792.

Karádi, V., Kozur, H.W., Görög, Á., 2013. Stratigraphically important lower Norian conodonts from the Csővár borehole (Csv-1), Hungary– Comparison with the conodont succession of the Norian GSSP candidate Pizzo Mondello (Sicily, Italy). In: Tanner, L.H., Spielmann, J.A., Lucas, S.G. (Eds.), The Triassic System. New Mexico Museum of Natural History and Science Bulletin, 61, pp. 284–295.

Karádi, V., Virág, A., Kolar-Jurkovšek, T., Jurkovšek, B., 2020. Stress-related evolution in Triassic Conodonts and the Middle Norian Juvenile Mortality. In: Guex, J., Torday, S., Miller Jr., W. (Eds.), Morphogenesis, Environmental Stress and Reverse Evolution. Springer, Cham. https://doi.org/10.1007/978-3-030-47279-5_4.

Karádi, V., Kolar-Jurkovšek, T., Gale, L., Jurkovšek, B., 2021. New advances in biostratigraphy of the lower/middle Norian transition: conodonts of the Dovško section, Slovenia. J. Earth Sci. 32 (3), 677–699.

Katvala, E.C., Stanley Jr., G.D., 2008. Conodont biostratigraphy and facies correlations in a late Triassic Island arc, Keku Strait, Southeast Alaska. In: Blodgett, R.B., Stanley Jr., G.D. (Eds.), The Terrane Puzzle: New Perspectives on Paleontology and Stratigraphy from the North American, vol. 442. Geological Society of America Special Paper, Cordillera, pp. 181–226. https://doi.org/10.1130/2008.442(11).

Kolar-Jurkovšek, T., Jurkovšek, B., 2010. New paleontological evidence of the Carnian strata in the Mežica area (Karavanke Mts, Slovenia): conodont data for the Carnian Pluvial Event. Palaeogeogr. Palaeoclimatol. Palaeoecol. 290, 81–88.
Kolar-Jurkovšek, T., Jurkovšek, B., 2019. Conodonts of Slovenia. Geological Survey of Slovenia, Ljubljana, p. 259.
Korte, C., Kozur, H.W., Bruckschen, P., Veizer, J., 2003. Strontium isotope evolution of late Permian and Triassic seawater. Geochim. Cosmochim. Acta 67, 47–62. https://doi.org/10.1016/S0016-7037(02)01035-9.
Kovács, S., Kozur, H., 1980. Stratigraphische Reichweite der wichtigsten Conodonten (ohne Zahnreihenconodonten) der Mittel- und Obertrias. Mitt. Geol. Paläontol. Innsbruck 10 (2), 47–78.
Kozur, H.W., 2003. Integrated ammonoid, conodont and radiolarian zonation of the Triassic. Hallesch Jahrb Geowissensch 25, 49–79.
Lei, J.Z.X., Husson, J.M., Golding, M.L., Orchard, M.J., Zonneveld, J.P., 2021. Stable carbon isotope record of carbonate across the Carnian–Norian boundary at the prospective GSSP section at Black Bear Ridge. British Columbia, Canada. Albertiana 46, 1–10.
Lei, J.Z.X., Golding, M.L., Husson, J.M., 2022. Paleoenvironmental interpretation of the late Triassic Norian – Rhaetian boundary interval in the Whitehorse Trough (Stikine Terrane, northern Canadian Cordillera). Palaeogeogr. Palaeoclimatol. Palaeoecol. 608, 111306 https://doi.org/10.1016/j.palaeo.2022.111306.
Lei, J.Z.X., Golding, M.L., Husson, J.M., 2024. Morphological trends across the Norian/Rhaetian boundary within late Triassic conodonts in western Canada: implications for protracted paleoenvironmental disturbance preceding the end-Triassic mass extinction. Paleobiology 50 (1), 85–95. https://doi.org/10.1017/pab.2023.30.
Liao, Z.T., Chen, Y.K., Wei, Z.H., Li, M.H., 2003. Tectonic evolution since late palaeozoic era in West Yunnan. J. Tongji Univ. 31, 1029–1033 (in Chinese with English abstract).
Lucas, S.G., 2010. The Triassic timescale an introduction. In: Lucas, S.G. (Ed.), The Triassic Timescale. Geological Society, London, pp. 1–16 (Special Publications 334).
Lucas, S.G., 2018. The Late Triassic timescale. In: The Late Triassic World. Springer, Cham, pp. 1–25. https://doi.org/10.1007/978-3-319-68009-5_1.
Lyu, Z., Golding, M.L., Zhao, H., Yao, H., Wang, X., Zhang, L., Li, Y., Han, C., 2024. Upper Triassic (middle Norian) conodont biostratigraphy succession from Qamdo, eastern Tibet. Palaeogeogr. Palaeoclimatol. Palaeoecol. 634, 111915 https://doi.org/10.1016/j.palaeo.2023.111915.
Mao, L., Tian, C.R., 1987. Late Triassic conodonts from the uppermost Mailonggang Formation in Mailonggang village of Lhünzhub County, Xizang (Tibet). China. Bull. Chin. Acad. Geol. Sci. 17, 159–168 (in Chinese with English abstract).
Maron, M., Rigo, M., Bertinelli, A., Katz, M.E., Godfrey, L., Zaffani, M., Muttoni, G., 2015. Magnetostratigraphy, biostratigraphy, and chemostratigraphy of the Pignola-Abriola section: new constraints for the Norian-Rhaetian boundary. Bull. Geol. Soc. Am. 127, 962–974.
Maron, M., Muttoni, G., Rigo, M., Gianolla, P., Kent, D.V., 2019. New magnetobiostratigraphic results from the Ladinian of the Dolomites and implications for the Triassic geomagnetic polarity timescale. Palaeogeogr. Palaeoclimatol. Palaeoecol. 517, 52–73. https://doi.org/10.1016/j.palaeo.2018.11.024.
Maron, M., Onoue, T., Satolli, S., Soda, K., Sato, H., Muttoni, G., Rigo, M., 2024. Weathering trends in the Norian through geochemical and rock magnetic analyses from the Pignola-Abriola Section (Lagonegro Basin, Italy). Clim. Past 20, 637–658.
Marzoli, A., Bertrand, H., Knight, K.B., Cirilli, S., Buratti, N., Vérati, C., Nomade, S., Renne, P.R., Youbi, N., Martini, R., Allenbach, K., Neuwerth, R., Rapaille, C., Zaninetti, L., Bellieni, G., 2004. Synchrony of the Central Atlantic magmatic province and the Triassic–Jurassic boundary climatic and biotic crisis. Geology 32, 973–976. https://doi.org/10.1130/G20652.1.
Mazza, M., Martínez-Pérez, C., 2015. Unravelling conodont (Conodonta) ontogenetic processes in the late Triassic through growth series reconstructions and X-ray icrotomography. Boll. Soc. Paleontol. Ital. 54 (3), 161–186.
Mazza, M., Furin, S., Spötl, C., Rigo, M., 2010. Generic turnovers of Carnian/Norian conodonts: climatic control or competition? Palaeogeogr. Palaeoclimatol. Palaeoecol. 290, 120–137.
Mazza, M., Cau, A., Rigo, M., 2012a. Application of numerical cladistic analyses to the Carnian–Norian conodonts: a new approach for phylogenetic interpretations. J. Syst. Palaeontol. 10 (3), 401–422.
Mazza, M., Nicora, A., Rigo, M., 2018. Metapolygnathus parvus Kozur, 1972 (Conodonta): a potential primary marker for the Norian GSSP (Upper Triassic). Boll. Soc. Paleontol. Ital. 57 (2), 81–101. https://doi.org/10.4435/BSPI.2018.06.
Mazza, M., Rigo, M., Gullo, M., 2012b. Taxonomy and stratigraphic record of the Upper Triassic conodonts of the Pizzo Mondello section (Western Sicily, Italy), GSSP candidate for the base of the Norian. Riv. Ital. Paleontol. Stratigr. 118, 85–130.
McRoberts, C.A., Newton, C.R., 1995. Selective extinction among end-Triassic European bivalves. Geology 23 (2), 102–104.
Metcalfe, I., 2006. Palaeozoic and Mesozoic tectonic evolution and palaeogeography of East Asian crustal fragments: the Korean Peninsula in context. Gondwana Res. 9, 24–46.
Moix, P.L., Kozur, H.W., Stampfli, G.M., Mostler, H., 2007. New paleontological, biostratigraphic and paleogeographic results from the Mersin Melange, SE Turkey. N. M. Mus. Nat. Hist. Sci. Bull. 41, 282–311.
Muttoni, G., Kent, D.V., Olsen, P.E., Stefano, P.D., Lowrie, W., Bernasconi, S.M., Hernández, F.T.M.N., 2004. Tethyan magnetostratigraphy from Pizzo Mondello (Sicily) and correlation to the late Triassic Newark astrochronological polarity time scale. Geol. Soc. Am. Bull. 116, 1043–1058. https://doi.org/10.1130/B25326.1.
Muttoni, G., Mazza, M., Mosher, D., Katz, M.E., Kent, D.V., Balini, M., 2014. A Middle–Late Triassic (Ladinian–Rhaetian) carbon and oxygen isotope record from the Tethyan Ocean. Palaeogeogr. Palaeoclimatol. Palaeoecol. 399, 246–259. https://doi.org/10.1016/j.palaeo.2014.01.018.
Ogg, J.G., Chen, Z.-Q., Orchard, M.J., Jiang, H.S., 2020. The Triassic Period. Geologic Time Scale 2020. Elsevier, pp. 903–953. https://doi.org/10.1016/B978-0-12-8243602.00025-5.
Onoue, T., Sato, H., Yamashita, D., Ikehara, M., Yasukawa, K., Fujinaga, K., Kato, Y., Matsuoka, A., 2016a. Bolide impact triggered the late Triassic extinction event in equatorial Panthalassa. Sci. Rep. 6, 29609. https://doi.org/10.1038/srep29609.
Onoue, T., Zonneveld, J.-P., Orchard, M.J., Yamashita, M., Yamashita, K., Sato, H., Kusaka, S., 2016b. Paleoenvironmental changes across the Carnian/Norian boundary in the Black Bear Ridge section, British Columbia, Canada. Palaeogeogr. Palaeoclimatol. Palaeoecol. 441, 721–733.
Onoue, T., Yamashita, K., Fukuda, C., Soda, K., Tomimatsu, Y., Abate, B., Rigo, M., 2018. Sr isotope variations in the Upper Triassic succession at Pizzo Mondello, Sicily: constraints on the timing of the Cimmerian Orogeny. Palaeogeogr. Palaeoclimatol. Palaeoecol. 499, 131–137.
Onoue, T., Michalík, J., Shirozu, H., Yamashita, M., Yamashita, K., Kusaka, S., Soda, K., 2022. Extreme continental weathering in the northwestern Tethys during the end Triassic mass extinction. Palaeogeogr. Palaeoclimatol. Palaeoecol. 594, 110934.
Orchard, M.J., 1983. Epigondolella populations and their phylogeny and zonation in the Upper Triassic. Fossils Strata 15, 177–192.
Orchard, M.J., 1991a. Upper Triassic conodont biochronology and new index species from the Canadian Cordillera. Pp. 299–335. In: Orchard, M.J., McCracken, A.D. (Eds.), Ordovician to Triassic Conodont Paleontology of the Canadian Cordillera, 417. Geological Survey of Canada, Bulletin, pp. 299–335.
Orchard, M.J., 1991b. Late Triassic conodont biochronology and biostratigraphy of the Kunga Group, Queen Charlotte Islands, British Columbia. In: Woodsworth, G.W. (Ed.), Evolution and Hydrocarbon Potential of the Queen Charlotte Basin, British Columbia, 1990–10. Geol. Surv. Can. Pap, pp. 173–193.
Orchard, M.J., 2006. Late Paleozoic and Triassic conodont faunas of Yukon Territory and northern British Columbia and implications for the evolution of the Yukon-Tanana terrane. In: Colpron, N. (Ed.), Paleozoic Evolution and Metallogeny of Pericratonic Terranes at the Ancient Pacific Margin of North America, Canadian and Alaskan Cordillera, 45. Geological Association of Canada, Special Paper, pp. 229–260.
Orchard, M.J., 2014. Conodonts from the Carnian-Norian Boundary (Upper Triassic) of Black Bear Ridge, Northeastern British Columbia, Canada. N. M. Mus. Nat. Hist. Sci. Bull. 64, 1–139.
Orchard, M.J., 2018. In: Over, D.J., Henderson, C.M. (Eds.), The Lower-Middle Norian (Upper Triassic) Boundary: New conodont taxa and a refined zonation. Conodont Studies Dedicated to the Careers and Contributions of Anita Harris, Glenn Merrill, Carl Rexroad, Walter Sweet, and Bruce Wardlaw, 395–396. Bulletins of American Paleontology, pp. 165–193.
Orchard, M.J., 2019. The Carnian-Norian boundary GSSP candidate at Black Bear Ridge, British Columbia, Canada: update, correlation, and conodont taxonomy. Albertiana 45, 50–68.
Orchard, M.J., Carter, E.S., Lucas, S.G., Taylor, D.G., 2007a. Rhaetian (Upper Triassic) condonts and radiolarians from New York Canyon, Nevada, USA. Albertiana 35, 59–65.
Orchard, M.J., Whalen, P.A., Carter, E.S., Taylor, H.J., 2007b. Latest Triassic conodonts and radiolarian-bearing successions in Baja California Sur. In: Lucas, S.G., Spielmann, J.A. (Eds.), The Global Triassic. New Mexico Museum of Natural History and Science Bulletin, 41, pp. 355–365.
Pan, G.T., Xu, Q., Hou, Z.Q., Wang, L.Q., Du, D.X., Mo, X.X., Li, D.M., Wang, M.J., Li, X. Z., Jiang, X.S., Hu, Y.Z., 2006. Metallogenic System and Resource Evaluation of Multiisland Arc Orogenic Process in the “Sanjiang” Area in Southwest China. Geological Publishing House, Beijing, pp. 1–420 (in Chinese).
Preto, N., Kustatscher, E., Wignall, P.B., 2010. Triassic climates – State of the art and perspectives. Palaeogeogr. Palaeoclimatol. Palaeoecol. 290, 1–10. https://doi.org/10.1016/j.palaeo.2010.03.015.
Preto, N., Agnini, C., Rigo, M., Sprovieri, M., Westphal, H., 2013. The calcareous nannofossil Prinsiosphaera achieved rock-forming abundances in the latest Triassic of western Tethys: consequences for the $\delta^{13}C$ of bulk carbonate. Biogeosciences 10 (9), 6053–6068.
Prokoph, A., El Bilali, H., Ernst, R., 2013. Periodicities in the emplacement of large igneous provinces through the Phanerozoic: relations to ocean chemistry and marine biodiversity evolution. Geosci. Front. 4, 263–276.
Que, G.M., Chen, D.M., Zhang, L.S., Xia, W.C., Zhu, C.Y., 1998. Lanping – Simao basin copper deposit. Geological Publishing House, Beijing, pp. 1–109 (in Chinese).
Rigo, M., Joachimski, M.M., 2010. Palaeoecology of late Triassic conodonts: constraints from oxygen isotopes in biogenic apatite. Acta Palaeontol. Pol. 55, 471–478.
Rigo, M., De Zanche, V., Mietto, P., Preto, N., Roghi, G., 2005. Biostratigraphy of the Calcari con Selce formation. Boll. Soc. Geol. Ital. 124, 293–300.
Rigo, M., Trotter, J.A., Preto, N., Williams, I.S., 2012a. Oxygen isotopic evidence for late Triassic monsoonal upwelling in the northwestern Tethys. Geology 40 (6), 515–518.
Rigo, M., Preto, N., Franceschi, M., Guaiumi, C., 2012b. Stratigraphy of the Carnian-Norian Calcari con Selce Formation in the Lagonegro Basin, Southern Apennines. Riv. Ital. Paleontol. Stratigr. 118, 143–154.
Rigo, M., Bertinelli, A., Concheri, G., Gattolin, G., Godfrey, L., Katz, M.E., Maron, M., Mietto, P., Muttoni, G., Sprovieri, M., Stellin, F., Zaffani, M., 2016. The PignolaAbriola section (southern Apennines, Italy): a new GSSP candidate for the base of the Rhaetian Stage. Lethaia 49 (3), 287–306.
Rigo, M., Mazza, M., Karádi, V., 2018. New Upper Triassic conodont biozonation of the Tethyan Realm. In: Tanner, L.H. (Ed.), The Late Triassic World: Earth in a Time of Transition, 46, pp. 189–235. https://doi.org/10.1007/978-3319-68009-5_6.
Rigo, M., Onoue, T., Tanner, L.H., Lucas, S.G., Godfrey, L., Katz, M.E., Zaffani, M., Grice, K., Cesar, J., Yamashita, D., Maron, M., Tackett, L.S., Campbell, H., Tateo, F., Concheri, G., Agnini, C., Chiari, M., Bertinelli, A., 2020. The Late Triassic Extinction

at the Norian/Rhaetian boundary: biotic evidence and geochemical signature. Earth Sci. Rev. 204, 103180.
Rigo, M., Jin, X., Godfrey, L., Katz, M.E., Sato, H., Tomimatsu, Y., Zaffani, M., Maron, M., Satolli, S., Concheri, G., Cardinali, A., Wu, Q.W., Du, Y.X., Lei, J.Z.X., van Wieren, C. S., Tackett, L.S., Campbell, H., Bertinelli, A., Onoue, T., 2024. Unveiling a new oceanic anoxic event at the Norian/Rhaetian boundary (Late Triassic). Sci. Rep. 14, 15574. https://doi.org/10.1038/s41598-024-66343-z.
Saltzman, M.R., Thomas, E., 2012. Carbon isotope stratigraphy. In: The Geologic Time Scale 2012. Elsevier, pp. 207–233. https://doi.org/10.1016/B978-0-444-59425-9.00011-1.
Sato, H., Onoue, T., Nakamura, T., 2010. Impact Spherules and Ni-rich Spinels in an Upper Triassic (Norian) Deep-Sea Deposit from Japan. Meteoritics Planet Sci. Suppl. 73, 5081.
Sato, H., Onoue, T., Nozaki, T., Suzuki, K., 2013. Osmium isotope evidence for a large late Triassic impact event. Nat. Commun. 4, 2455. https://doi.org/10.1038/ncomms3455.
Sato, H., Shirai, N., Ebihara, M., Onoue, T., Kiyokawa, S., 2016. Sedimentary PGE signatures in the late Triassic ejecta deposits from Japan: implications for the identification of impactor. Palaeogeogr. Palaeoclimatol. Palaeoecol. 442, 36–47.
Sato, H., Ishikawa, A., Onoue, T., Tomimatsu, Y., Rigo, M., 2021. Sedimentary record of Upper Triassic impact in the Lagonegro Basin, southern Italy: insights from highly siderophile elements and Re-Os isotope stratigraphy across the Norian/Rhaetian boundary. Chem. Geol. 586, 120506 https://doi.org/10.1016/j.chemgeo.2021.120506.
Sato, H., Nozaki, T., Onoue, T., Ishikawa, A., Soda, K., Yasukawa, K., Kimura, J.I., Chang, Q., Kato, Y., Rigo, M., 2023. Rhenium-osmium isotope evidence for the onset of volcanism in the central Panthalassa Ocean during the Norian "chaotic carbon episode". Glob. Planet. Chang. 229, 104239 https://doi.org/10.1016/j.gloplacha.2023.104239.
Scotese, C.R., 2021. An atlas of phanerozoic paleogeographic maps: the seas come in and the seas go out. Annu. Rev. Earth Planet. Sci. 49, 679–728.
Shi, Z., Jin, X., Preto, N., Rigo, M., Du, Y., Han, L., 2019. The Carnian Pluvial Episode at Ma'antang, Jiangyou in Upper Yangtze Block, Southwestern China. J. Geol. Soc. 176 (1), 197–207. https://doi.org/10.1144/jgs2018-038.
Sussman, A.J., Weil, A.B., 2004. Orogenic curvature: integrating paleomagnetic and structural analyses. Geol. Soc. Am. Spec. Pap. 383, 1–271.
Swart, P.K., 2015. The geochemistry of carbonate diagenesis: the past, present and future. Sedimentology 62 (5), 1233–1304.
Tanner, L.H., 2018. Climates of the Late Triassic: Perspectives, proxies and problems. In: The Late Triassic World. Springer, Cham, pp. 59–90. https://doi.org/10.1007/978-3-319-68009-5_3.
Todaro, S., Rigo, M., Tackett, L., Di Stefano, P., 2023. Evidence of a biodiversity crisis documented on a peritidal carbonate succession from western Tethys (Sicily): new data on the End Triassic Mass Extinction. Ital. J. Geosci. 142 (1), 122–130. https://doi.org/10.3301/IJG.2023.04.
Tomimatsu, Y., Nozaki, T., Sato, H., Takaya, Y., Kimura, J.I., Chang, Q., Naraoka, H., Rigo, M., Onoue, T., 2021. Marine osmium isotope record during the Carnian "pluvial episode" (Late Triassic) in the pelagic Panthalassa Ocean. Glob. Planet. Chang. 197, 103387.
Tomimatsu, Y., Nozaki, T., Onoue, T., Matsumoto, H., Sato, H., Takaya, Y., Kimura, J.I., Chang, Q., Rigo, M., 2023. Pelagic responses to oceanic anoxia during the Carnian Pluvial Episode (Late Triassic) in Panthalassa Ocean. Sci. Rep. 13 (1), 16316.
Tong, Z.D., 2018. Metallogenesis of the Bijiashan Antimony Orefield in Weishan County, Western Yunnan Province. China University of Geosciences, Beijing, pp. 1–142 (in Chinese with English abstract).
Tong, J.N., Chu, D.L., Miao, X., Shu, W.C., Guo, W.W., Wu, Y.Y., Su, Y., Wu, K., Ji, K.X., Yu, Y.Y., 2021. Lithostratigraphic subdivision and correlation of the Triassic in China. J. Stratigr. 45 (3), 340–363.
Trotter, J.A., Williams, I.S., Nicora, A., Mazza, M., Rigo, M., 2015. Long-term cycles of Triassic climate change: a new δ18O record from conodont apatite. Earth Planet. Sci. Lett. 415, 165–174. https://doi.org/10.1016/j.epsl.2015.01.038.
Usuki, T., Lan, C.Y., Wang, K.L., Chiu, H.Y., 2013. Linking the Indochina block and Gondwana during the Early Paleozoic: evidence from U–Pb ages and Hf isotopes of detrital zircons. Tectonophysics 586, 145–159. https://doi.org/10.1016/j.tecto.2012.11.010.
van Soest, M.C., Hodges, K.V., Wartho, J.-A., Biren, M.B., Monteleone, B.D., Ramezani, J., Spray, J.G., Thompson, L.M., 2011. (U-Th)/He dating of terrestrial impact structures: the Manicouagan example. Geochem. Geophys. Geosyst. 12, Q0AA16. https://doi.org/10.1029/2010GC003465.
Vrielynck, B., 1987. Conodontes du Trias Perimediterraneen. Systematique, Stratigraphie. Documents des Laboratoires de Géologie Lyon, 97, pp. 1–301.
Wang, Z.H., Dong, Z.Z., 1985. Discovery of conodont *Epigondolella* fauna from Late Triassic in Baoshan area, western Yunnan. Acta Micropalaeontol. Sin. 2 (2), 125–132 (in Chinese with English abstract).
Wang, C.Y., Lang, J.B., 2019. Triassic stages and conodont biostratigraphy. Glob. Geol. 38 (1), 20–33 (in Chinese with English abstract).
Wang, Q., Deng, J., Li, C., Li, G., Yu, L., Qiao, L., 2014. The boundary between the Simao and Yangtze blocks and their locations in Gondwana and Rodinia: constraints from detrital and inherited zircons. Gondwana Res. 26 (2), 438–448. https://doi.org/10.1016/j.gr.2013.10.002.
Wang, X.D., Du, Y.X., Shi, Z.Q., Chen, B., 2019. Characteristics of conodonts and sedimentary environment of upper Norian Nanshuba and Dashuitang formations in Baoshan, Yunnan province. Acta Palaeontol. Sin. 58 (1), 79–91 (in Chinese with English abstract).
Wen, H.X., Shi, H., Wang, D.Y., 2011. New information and geological sense of bivalve fossils from the Waigucun Formation in southeast of the Simao basin, Yunnan, China. Geol. Bull. China 30 (1), 179–183 (In Chinese with English abstract).
Whiteside, J.H., Ward, P.D., 2011. Ammonoid diversity and disparity track episodes of chaotic carbon cycling during the early Mesozoic. Geology 39, 99–102. https://doi.org/10.1130/G31401.1.
Whiteside, J.H., Olsen, P.E., Eglinton, T., Brookfield, M.E., Sambrotto, R.N., 2010. Compound-specific carbon isotopes from Earth's largest flood basalt eruptions directly linked to the end-Triassic mass extinction. Proc. Natl. Acad. Sci. USA 107 (15), 6721–6725. https://doi.org/10.1073/pnas.1001706107.
Wu, G.C., Ji, Z.S., Lash, G.G., Yao, J.X., 2021. The Upper Triassic deposits of the west Bangong-Nujiang Suture Zone and their palaeogeographic implications. Sci. Rep. 11, 19509.
Wu, Q.W., Du, Y.X., Jin, X., Shi, Z.Q., 2022. Conodont biostratigraphy and sedimentary facies of the Sanhedong Formation (Norian, Upper Triassic) in Weishan, western Yunnan Province. Acta Palaeontol. Sin. 61 (1), 51–64 (in Chinese with English abstract).
Wu, G.C., Ji, Z.S., Lash, G.G., Yao, J.X., 2023. Norian conodonts of the South Qiangtang Terrane, North Tibet, and their palaeogeographic implications. Palaeogeogr. Palaeoclimatol. Palaeoecol. 613, 111402.
Yamashita, D., Kato, H., Onoue, T., Suzuki, N., 2018. Integrated Upper Triassic Conodont and Radiolarian Biostratigraphies of the Panthalassa Ocean. Paleontol. Res. 22 (2), 167–197.
Yang, L., Wang, Q., Wang, Y., Li, G., 2018. Proto-to Paleo-Tethyan evolution of the eastern margin of Simao block. Gondwana Res. 62, 61–74. https://doi.org/10.1016/j.gr.2018.02.012.
Zaffani, M., Agnini, C., Concheri, G., Godfrey, L., Katz, M., Maron, M., Rigo, M., 2017. The Norian "chaotic carbon interval": new clues from the δ13C org record of the Lagonegro Basin (southern Italy). Geosphere 13 (4), 1133–1148.
Zaffani, M., Jadoul, F., Rigo, M., 2018. A new Rhaetian $\delta^{13}C_{org}$ record: carbon cycle disturbances, volcanism, End-Triassic mass Extinction (ETE). Earth Sci. Rev. 178, 92–104. https://doi.org/10.1016/j.earscirev.2018.01.004.
Zeng, W.P., Purnell, M.A., Jiang, H.S., Zang, M.H., 2021. Late Triassic (Norian) conodont apparatuses revealed by conodont clusters from Yunnan Province, Southwestern China. J. Earth Sci. 32 (3), 709–724. https://doi.org/10.1007/s12583-021-1459-2.
Zeng, W.P., Jiang, H.S., Chen, Y., Ogg, J., Zhang, M.H., Dong, H.X.S., 2023. Upper Norian conodonts from the Baoshan block, western Yunnan, southwestern China, and implications for conodont turnover. PeerJ 11, e14517. https://doi.org/10.7717/peerj.14517.